



MASTER THESIS REPORT

Versatile Microfluidic Circulation to Evaluate Tumor Cross-talk Using a Multi-Organ-on-Chip Approach

Luuk van de Schepop

Applied Microfluidics for BioEngineering Research (AMBER)
Faculty of Science & Technology (TNW)
University of Twente, The Netherlands

Committee:

Dr. A. Zuchowska (Daily Supervisor)
Prof. Dr. Ir. S. Le Gac (Committee Chair)
Prof. Dr. L.W.W.M. Terstappen (External Member)

11 January 2021

UNIVERSITY OF TWENTE.

Abstract

Breast cancer is the most common cancer among women. Cancer metastases often determine the severity of the disease: rather than the primary tumor, cancer metastases account for 90% of cancer related death. Metastasis is a complex process depending on the primary tumor, the tumor microenvironment and secondary organs. Many distinct properties are required to establish successful dissemination. Rather than random distribution, tumor cells show organ preferential dissemination. This is partially explained by mechanical factors such as organ perfusability and shear stresses, but cellular and molecular processes, regarding both primary and secondary organ, play an important role as well. However, despite the evident clinical importance of metastasis research, knowledge on the biological processes involved in metastasis is limited. Current research focuses on mimicking the metastatic cascade *in vitro*. What is still missing, however, is a dynamic circulation that mimics all steps in the metastatic cascade and thus the complexity of tumor progression.

Here, an automated circulation that is compatible with multiple organ-on-a-chip models is presented. The circulation can provide unidirectional flow and physiological shear stresses. By re-circulating medium, cross-talk between organs can be established. Sampling of the circulation can be performed on-demand for cellular and molecular analysis to eventually gain insight into the cross-organ communication processes. HEPES buffering is used to maintain culture conditions outside a conventional incubator. The efficiency and cytotoxicity of HEPES buffering is assessed first in 2D culture for all associated cell types. A vessel mimicking organ module is presented that is compatible with the circulation. The vessel module consists of a collagen hydrogel with a cylindrical lumen coated with endothelial cells. Viability and morphology is examined for both static vessel models and models subjected to shear corresponding to a flow of 30 $\mu\text{L}/\text{min}$. Morphological changes are observed for endothelium subjected to shear for 24 h, that are associated with better reproduction of the *in vivo* behavior of endothelium. Additionally, a future design aimed to recapitulate the breast tumor microenvironment, that is compatible with the circulation, is discussed. These results demonstrate the efficacy of the circulation as a promising tool to study cancer metastasis, but also display the versatility of the circulation to be used for a wide variety of conditions comprising organ cross-talk.

Samenvatting

Borstkanker is de meest voorkomende kanker onder vrouwen. Kankermetastasen bepalen in de meeste gevallen hoe dodelijk de ziekte is: in 90% van dodelijke gevallen van kanker komt dit door de metastasen. Metastasering is een complex proces, niet alleen afhankelijk van de primaire tumor, maar ook van de lokale omgeving en secundaire organen. Tumor cellen hebben zeer specifieke eigenschappen nodig om succesvol te kunnen metastaseren van primair naar secundair orgaan. Deze metastasering is in vele gevallen orgaan specifiek. Gedeeltelijk is dit te verklaren door mechanische factoren zoals mate van perfusie in het betreffende orgaan en schuifspanning, maar ook cellulaire en moleculaire processen spelen een aanzienlijke rol. Ondanks de klinische relevantie van onderzoek naar de onderliggende processen van metastasen, is de kennis nog steeds beperkt. Huidig onderzoek richt zich op het nabootsen van onderdelen van de metastatische cascade *in vitro*. Er mist echter tot op heden een platform dat alle stappen in de metastatische cascade succesvol kan nabootsen, en daarmee dus de complexiteit van tumor progressie kan recapituleren.

In dit verslag is een geautomatiseerde circulatie ontwikkeld, die compatibel is met meerdere orgaan-onchip modellen. De circulatie zorgt voor uni-directionele vloeistofstroom en fysiologische schuifspanning. Cel medium wordt hergebruikt, zodat orgaan tot orgaan communicatie kan worden bewerkstelligd. Bemonstering van de circulatie kan op aanvraag worden uitgevoerd voor cellulaire en moleculaire analyse, om uiteindelijk inzicht te krijgen in de communicatie die plaatsvindt. HEPES buffer is gebruikt om CO₂-onafhankelijk medium te verkrijgen. Voor alle celtypen relevant voor borstkanker is de efficiëntie en toxiciteit van HEPES getest in 2D kweek. Een bloedvat model, dat compatibel is met de circulatie, is gepresenteerd. Deze bestaat uit een collageen hydrogel waarin een cilindrisch lumen gecoat is met endotheel. Levensvatbaarheid en morfologie is getest voor statische en mechanisch gestimuleerde modellen met een stroomsnelheid van 30 $\mu\text{L}/\text{min}$. Er is een duidelijke verandering in morfologie geobserveerd voor cellen die voor 24 h onder stress werden gekweekt. Dit wordt geassocieerd met betere reproductie van *in vivo* gedrag van endotheel. Daaropvolgend is een design gepresenteerd dat borstkanker kan recapituleren. De resultaten demonstreren de potentie van de circulatie als veelbelovende tool om kankermetastasen te bestuderen. Daarnaast is de veelzijdigheid van de circulatie benadrukt, aangezien de circulatie voor een grote verscheidenheid van ziekten waarin orgaancommunicatie een rol speelt ingezet kan worden.

Table of Contents

1	Introduction	5
1.1	Breast cancer.....	5
1.2	Tumor metastasis	5
1.3	<i>In vitro</i> disease models	7
1.4	State-of-the-art.....	8
1.5	Remaining problem	16
2	Aim & Requirements.....	17
2.1	Aim.....	17
2.2	Circulation requirements.....	17
3	Materials & Methods	18
3.1	Organ-on-a-chip fabrication	18
3.2	Cell culture & seeding.....	21
3.3	HEPES buffer concentration optimization	22
3.4	Circulation design & optimization	23
3.5	Providing shear conditions	25
3.6	Breast tumor-on-a-chip characterization	26
3.7	Imaging	26
3.8	Statistics	26
3.9	Image processing	26
4	Results & Discussion	27
4.1	HEPES buffer concentration optimization	27
4.2	Circulation optimization	31
4.3	Providing shear conditions	35
4.4	Breast tumor-on-a-chip characterization	39
5	Conclusions	41
6	Outlook	42
7	Acknowledgements	45
8	References	46
9	Supplementary data	50

1 Introduction

1.1 Breast cancer

Breast cancer is the most common cancer among women, and the second most common cancer worldwide, accounting for an estimated 28.2% of all female cancer cases in Europe in 2018. [1, 2] 2.1 million new breast cancer cases are reported each year. [3] Rather than the primary tumor, secondary malignant growths (metastases) often determine the severity of the disease. Cancer related death is in 90% of cases due to metastases. [4]

1.2 Tumor metastasis

The metastatic cascade is known to involve many steps including invasion of the basal membrane, intravasation, circulation, and extravasation followed by dormancy and growth at the distant tumor site. [5] An overview of the metastatic cascade for breast cancer to bone marrow is shown in Figure 1. A tumor cell requires many distinct features to metastasize. A tumor cell has to be able to detach from the primary tumor, intravasate into the bloodstream, withstand shear and collisions and interactions with blood cells, extravasate into the secondary organ, invade the local environment and grow at the target organ. Therefore, no more than 0.01% of the circulating tumor cells (CTCs) is able to form secondary lesions. [6]

1.2.1 Organ-specificity

Interestingly, metastases have an organ-specific nature. This means that primary tumors show an increased affinity to metastasize to specific organs. For breast cancer, metastases are most frequently found in bone, liver, brain and lung tissue. [7, 8] This is partly explained by the fact that some organs show increased perfusion or geometrically favorable attributions. Flow patterns in the blood circulation therefore account for roughly 40% of organ-specificity. [9] A lot of recent theories aim to explain the organ-specific nature of tumor cell dissemination, and describe effects besides flow patterns in the blood circulation. The focus of these studies is not only on the primary tumor but also on the distinct properties and behavior of the target organ. Tumor cell ("seed") and target organ ("soil") behavior is frequently described as key to dissemination. [10] This "seed and soil" principle was first described by Stephen Paget in 1889. [11] Metastasis is thus a complex process depending on the primary tumor, the tumor microenvironment (TME) and target organs. This thesis focuses mainly on breast tumor metastasis to bone marrow.

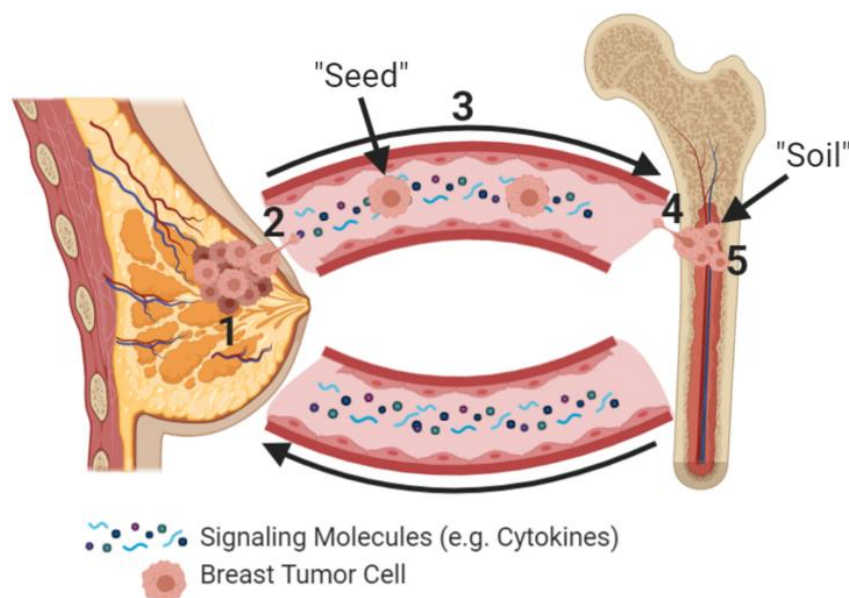


Figure 1: Overview of the metastatic cascade for breast cancer cells invading the bone. 1: Cells proliferate at the primary site. 2: Cells invade the basal membrane, and intravasate into the surrounding vasculature. 3: Cells, once intravasated, circulate in the bloodstream (now called circulating tumor cells, CTCs). 4: Cells home and extravasate at the distant organ. 5: Growth at the secondary site. Signaling molecules possibly play a role in tumor progression. Created using BioRender.

1.2.2 “Seed” and “Soil” factors

Soil factors can be categorized as primary and secondary soil factors. Primary soil factors are factors of the TME surrounding the primary tumor. Primary soil factors include vascularization (endothelial cell communication) and recruitment of the immune system. The way cancer cells behave is greatly influenced by stromal components such as fibroblasts, endothelial cells, immune cells, adipocytes, and extracellular matrix. Fibroblasts, the most abundant cell type in breast cancer, are pro-tumorigenic and can transform into cancer associated-fibroblasts (CAFs). CAFs play a major role in development of fibrotic tissue and resistance to treatment. [12] Additionally, macrophages play a major role in tumor proliferation, as they tune processes such as angiogenesis, inflammation, and tissue remodeling and repair. [13]

The so-called “secondary soil” consists of many factors and cell types, capable to promote colonization and metastasis growth. [14] Firstly, a very important factor influencing organ preference of metastatic spread is the anatomy of the endothelial lineage. For bone, one of the key components of metastasis is the presence of fenestrations. Fenestrations allow traffic of hematopoietic cells, but can also be exploited by tumor cells to extravasate into the bone tissue. In addition, selective attachment of tumor cells to the bone environment due to mutations of the primary tumor can cause receptor-mediated extravasation. A lot of these mutations are already described in literature and illustrated below in Figure 2. [15, 16] For example, chemo-attracting factors secreted by osteoblasts are known to recruit cancer cells. Chemokines known to be secreted by the bone such as CXCL5 and CXCL12 promote the exit of cancer cells into bone marrow cavities (Figure 2). Cancer cells with specific mutations are capable to metastasize to bone by replicating receptors CXCR2, CXCR4 and CXCR7 to use hematopoietic progenitor cell vascular exit strategies. Other factors mediating cellular adhesion include integrin $\alpha 5\beta 3$, Annexin II and the Jagged ligand. [17] However, despite the evident clinical importance of metastasis research, knowledge on the biology of cellular and molecular processes involved in metastasis is limited. [5, 7]

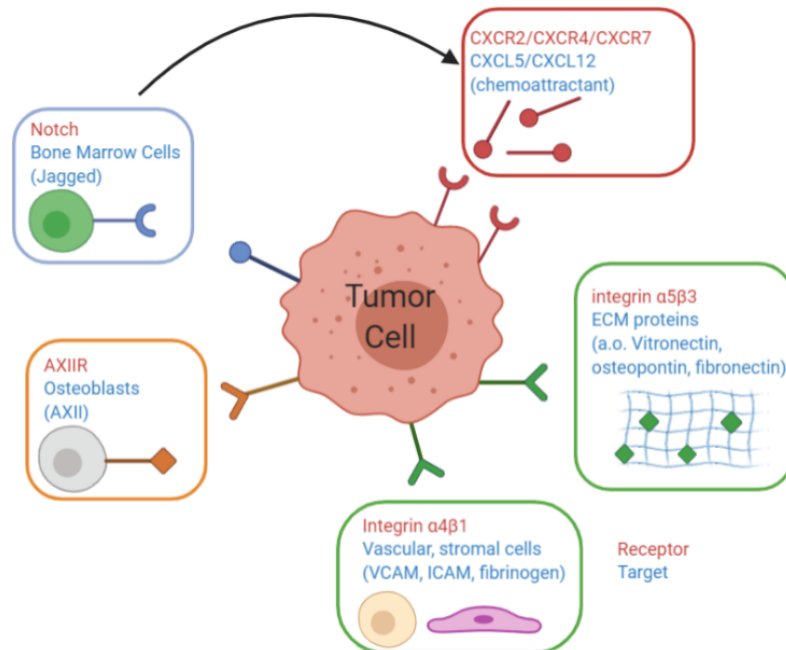


Figure 2: Overview of bone-specific factors involved in tumor cell attraction for specific mutations of the tumor cell. Created using BioRender.

1.3 *In vitro* disease models

A major challenge for tumor drug development is the establishment of relevant disease models. Simple prediction models of drug properties cannot easily be extrapolated to the human physiology. Currently, less than 10% of drugs for cancer treatment reach the medical market. [18] A lot of those drugs show good potential in pre-clinical tests. [18] This implies that the predictability of current models is too low. Progress is thus needed to find new cost-effective treatments. [19]

1.3.1 Standard models

Already established models include *in vitro* cell culture systems. For instance, 2D cell culturing allows fast, simple, reproducible, and cheap drug testing. [15, 18] To obtain a physiologically relevant model, however, 2D cell cultures have to be replaced by other culturing methods. [18, 20] For instance, 3D cultures bring improvements in morphology, implementation of multiple cell types, and relevant diffusion kinetics due to the presence of gradients. Mimicking transport mechanisms is unfortunately not possible, as perfusion of the culture is mostly limited. Thus, to obtain a functioning tumor niche, aspects such as vasculature and blood flow have to be considered. An alternative is use of *in vivo* animal models, which still remains the gold standard, as aspects such as organ-organ cross-talk and effects on side-organs can be assessed. However, translational issues regarding animal-to-human deviations, ethical concerns, high cost, and poor time efficacy decrease the suitability of animal models for drug research. [20]

1.3.2 Organ-on-a-chip models

Aiming to improve upon the static nature of 3D culture models, the first functioning organ-on-a-chip (OoC) was introduced in 2007. [21] An OoC model provides an *in vitro* platform which combines tissues to pave the way towards physiological reproduction of living tissue. Advanced OoC models make it possible to spatially organize human or even patient-derived cells as well as to implement a variety of physical and biochemical cues, and gradients thereof. Due to the small size, the system is cost-effective. Additionally, OoC systems could possibly be produced in a fast and reproducible fashion in the near future. [22, 23] Additionally, OoC systems reproduce multicellular interfaces of organs better compared to static 3D cultures.

1.3.3 Multi-organ-on-a-chip models

As discussed before, tumor metastasis is a complex process depending on interactions with multiple organs. Therefore, it would be beneficial to mimic not only tumor, but also target organ in an interconnected platform. Only then, the complexity of the disease can be modeled adequately. This so called multi-organ-on-a-chip technology is aimed to recapitulate complex interactions between organs. Only by implementing both organs in a single platform the cross-organ communication processes can be mimicked properly.

Some current research focuses on mimicking the organs involved in cancer metastasis. Both primary tumor and soil have been reported, as well as multi-organ platforms aimed to combine organ models to establish cross-talk. Some key papers are discussed below.

1.4 State-of-the-art

1.4.1 Breast tumor models

For example, a breast tumor-on-a-chip was reported by Nashimoto *et al.* [24] A vascularized 3D spheroid was cultured along with two blood vessels to obtain a vascular network (Figure 3A). These blood vessels were created using Human Umbilical Vein Endothelial Cells (HUVECs). A perfusable vascular network was established, enabling long-term perfusability (Figure 3B). Moreover, the importance of flow was highlighted by comparing a perfused model to a static model. Paclitaxel, an anti-cancer drug was added both in static and dynamic (flow) conditions, both with and without vasculature in the model. It was observed that without flow, the volume of the tumor spheroid decreases correlating to the concentration of paclitaxel (Figure 3C). However, in the presence of flow, at low concentrations of paclitaxel, the spheroid shows increased drug resistance. The volume of the spheroid is therefore not significantly lowered for low concentrations of paclitaxel (Figure 3D).

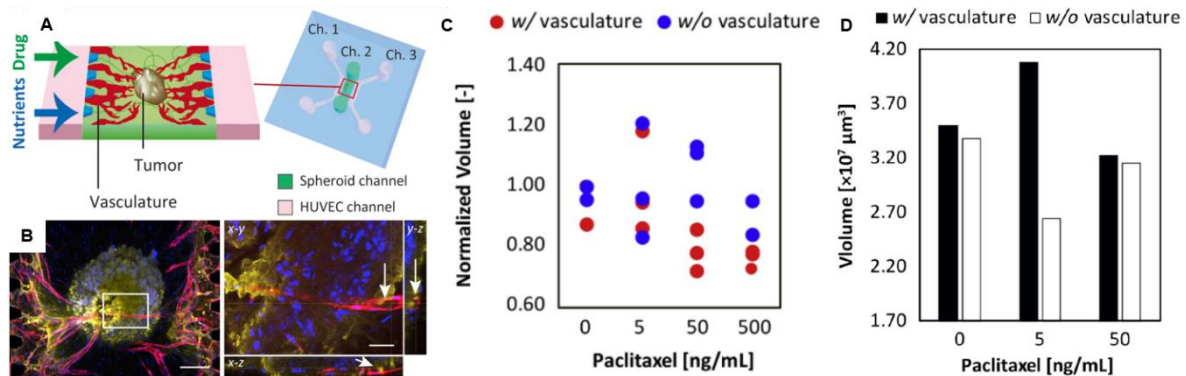


Figure 3: Vascularized breast tumor-on-a-chip model. A: schematic overview of the platform. A spheroid is introduced in the middle channel, surrounded by two HUVEC channels. B: Immunofluorescence images of the vascularized tumor spheroid. Red: HUVECs, yellow: E-cadherin, blue: nuclei. Scale bar: 200 μm . C: Spheroid volumes upon administration of 0, 5, and 50 ng/mL paclitaxel, both with and without vasculature (perfusion). At low concentrations of paclitaxel, the perfusion increased cellular proliferation, whereas for the static condition, the volume of the spheroid decreased. Adapted from [24].

Additionally, intravasation models have been reported, studying the invasion and intravasation of a tumor cell into the bloodstream. Nagaraju *et al.* [25] developed a platform capable to assess breast cancer cell intravasation as well as tumor-vascular cross-talk using three-layer cell-laden hydrogels (shown in Figure 4A). Breast cancer cells (in collagen) and endothelial cells (in fibrin) were separated using a collagen hydrogel stroma layer. It was demonstrated that the presence of both red fluorescent breast cancer cells (MDA-MB-231) and endothelial cells (HUVECs) resulted in neovascularization, enhancing tumor cell intravasation (shown in Figure 4B+C). This effect was not as evident in the absence of HUVECs. Furthermore, cytokines involved in angiogenesis were investigated and analyzed using ELISA (Figure 4D+E). Compared to other factors, a notable amount of VEGF ($>5000 \text{ pg/mL}$) was detected. For 6 of the 10 secreted proteins, there was no significant difference between samples with and without HUVECs. However, for the other 4 factors, there was a significant increase for samples containing both HUVECs and MDA-MB-231 cells compared to samples without HUVECs. This effect was also seen in absence of MDA-MB-231 cells, indicating that solely HUVECs secrete these angiogenesis related cytokines.

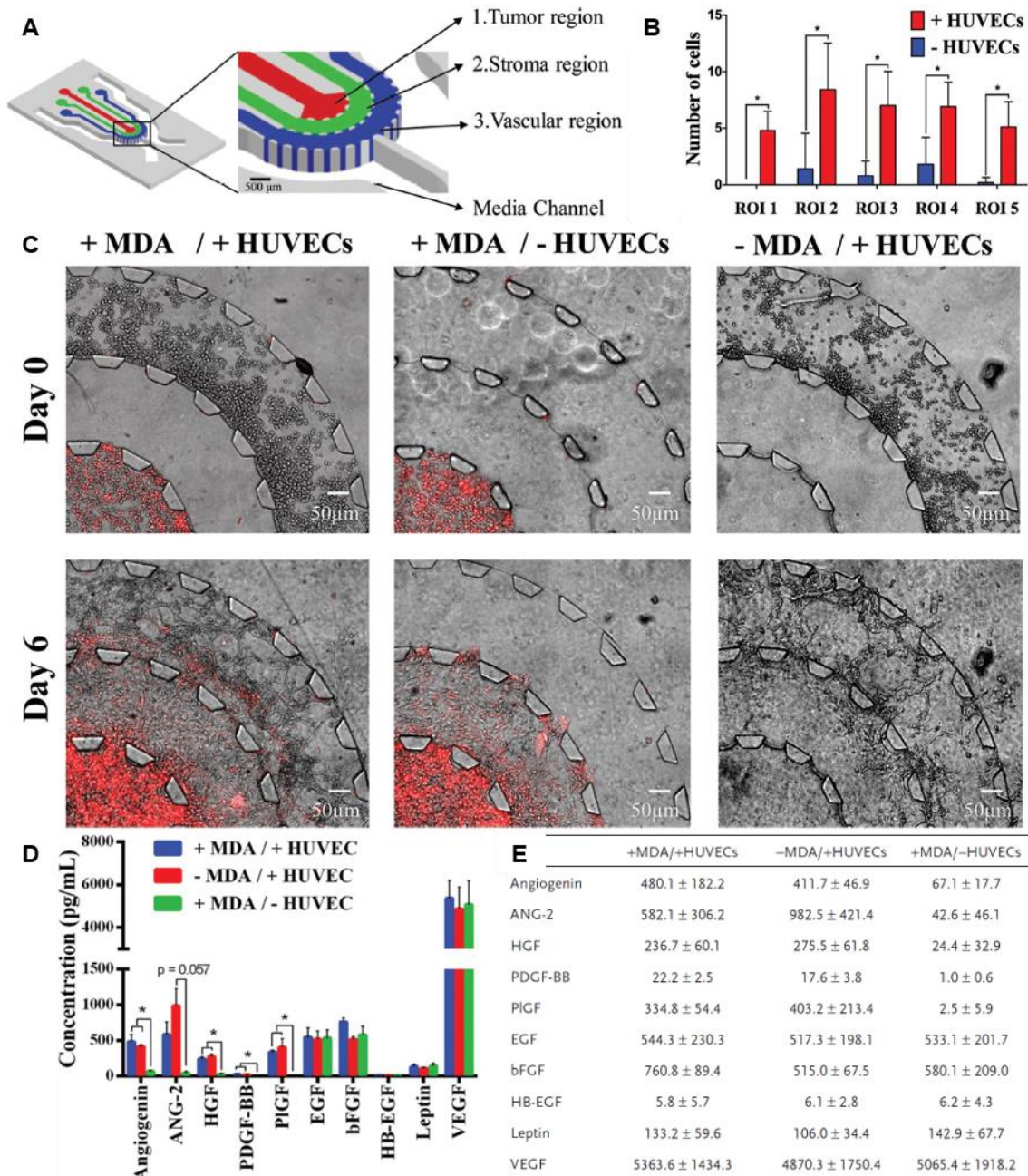


Figure 4: Overview of a breast cancer intravasation model. A: Schematic overview of the design B: Determination of the number of intravasated cells in several regions of interest (ROIs) in presence and absence of vasculature (HUVECs) C: Experimental setup for three conditions (containing MDA-MB-231 cells, HUVECs, or both) to model intravasation. MDA-MB-231 cells were fluorescently labeled with a red marker. It is shown that vasculature contributes to intravasation in the outer channel. D: ELISA comparison of angiogenic related factor concentrations of samples cultured with either HUVECs, MDA-MB-231 cells, or both at day 6 (* P < 0.05). E: Numerical values corresponding to D. Adapted from [25].

1.4.2 Bone models

Not only the breast tumor microenvironment is described and investigated. Some literature also focuses on mimicking the soil factors of the bone microenvironment. Bersini *et al.* [26] developed a tri-culture 3D *in vitro* model that mimics extravasation of human breast cancer cells to bone tissue. The OoC system is shown in Figure 5A. Bone specificity was shown by comparing extravasation in presence and absence of bone cells in a bone matrix, aligned with a lumen covered with endothelial cells. MDA-MB-231 breast cancer cells were introduced at a concentration of 50,000 cells/mL in the lumen and incubated for 1 h in static conditions. Afterwards, medium was replaced by medium lacking cells. Significant differences in both extravasation number and distance was observed (Figure 5B+C), showing that indeed bone cells contribute to breast cancer cell extravasation.

Furthermore, it was proven that cytokines CXCR2 and CXCL5 play a pivotal role in extravasation (Figure 5D+E). CXCR2 is a breast cancer cell surface receptor for the ligand CXCL5. It was first proven that CXCR2 was expressed by the cancer cells using an immunostaining in 2D culture. Furthermore, it was proven using an ELISA that CXCL5 was produced by the bone cells used in this experiment. Then, the addition of a CXCR2 blocking antibody (Figure 5D) and artificial addition of CXCL5 to a collagen matrix (Figure 5E) significantly altered the response of the cancer cells. This means that CXCR2 and CXCL5 play a pivotal role in breast tumor metastasis to bone.

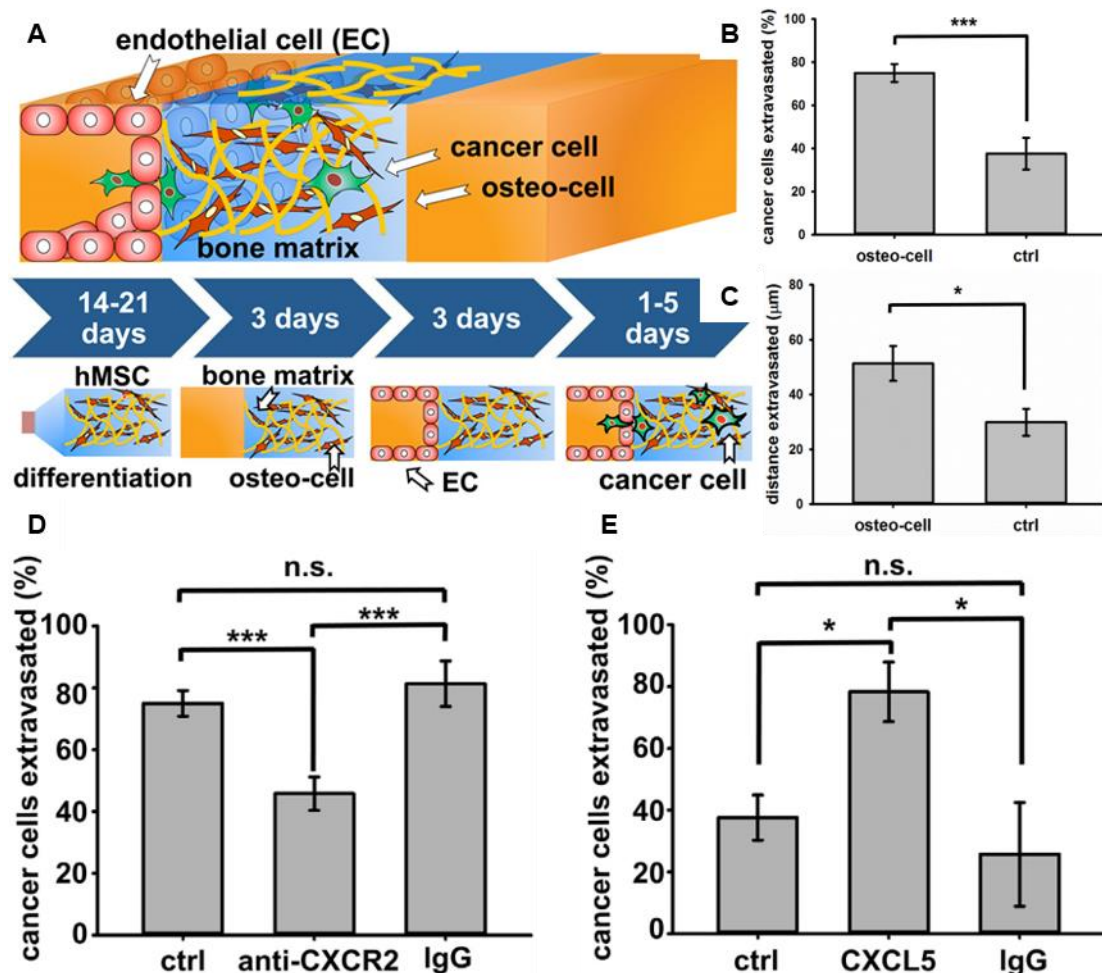


Figure 5: Overview of a breast cancer extravasation model. A: overview of the tri-culture system, with time scheme for generation of the microenvironment. B: Amount of cancer cells extravasated both in presence and absence of bone cells. C: The distance of cancer cell extravasation both in presence and absence of bone cells. D: Amount of cancer cells extravasated in presence of an CXCR2 inhibitor. E: Amount of cancer cells extravasated in presence of CXCL5 (* $P < 0.05$, *** $P < 0.005$). Adapted from [26].

A human bone model for studying breast cancer cell migration was presented by A. Marturano-Kruik et al. [27] A decellularized bone scaffold was first recellularized using bone marrow stem cells and endothelial cells. Then, the scaffold was integrated in a microfluidic device. Next, after formation of a vascular network under constant interstitial flow, cancer cells were introduced in the OoC. This condition was compared to a static condition. In Figure 6A below, an overview of the device is depicted, whereas Figure 6B+C presents results of the device for both static and flow conditions. A fourfold decrease in cancer cell growth rate was measured upon introduction of flow to the system (Figure 6B). Cancer cells introduced under flow entered a slow-proliferative state. This also explains why cells under flow are less affected by sunitinib (Figure 6C), a commonly used drug to target proliferative cancer cells and vasculature. This shows that the model correctly mimicked drug resistance of breast cancer cells colonizing bone. It was proposed that the bone model with interstitial flow promotes the formation of stable vasculature and mediates cancer cell colonization.

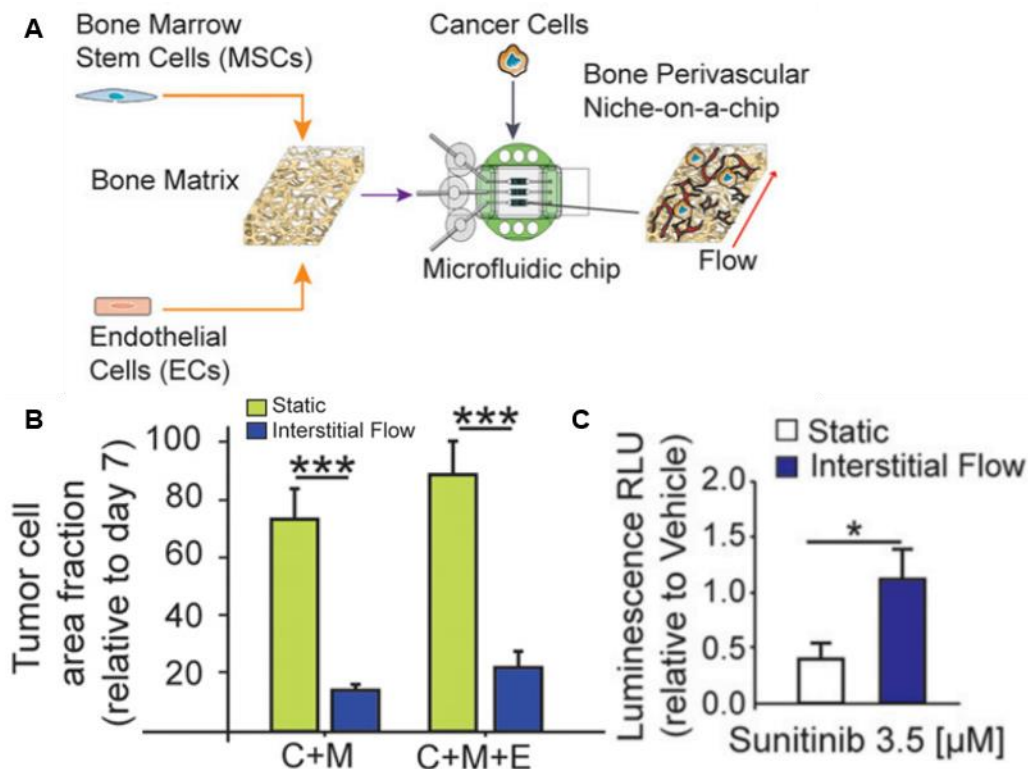


Figure 6: Overview of a perfused bone matrix model and accompanied results. A: Schematic overview of the bone perivascular niche-on-a-chip model. B: Comparison of total cancer cell area upon static and interstitial flow culturing conditions at day 14, in presence of cancer cells (C) and Mesenchymal stem cells (M) both with (C+M+E) and without (C+M) endothelial cell introduction. C: Effect of sunitinib to the total cell count, both in presence and absence of flow (* P < 0.05, *** P < 0.001). Adapted from [27].

Another Bone-Mimicking microenvironment established vasculature and interstitial flow using endothelial cells, osteoblasts, and mesenchymal stem cells. The device is shown in Figure 7A. By closing some of the outlets, flow is only able to move through the hydrogel, so that interstitial flow is mimicked. Figure 7B presents extravasation of MDA-MB-231 cells (in red) through endothelial cell vasculature (in green). Figure 7C presents cancer cell extravasation rate and vessel permeability in presence and absence of bone microenvironment. These results were compared to muscle microenvironment using C2C12 cells. Interestingly, bone microenvironment significantly increased cancer cell extravasation rate and vessel permeability. This could imply that vessel lineages are less densely formed due to the surrounding tissue, increasing extravasation efficacy. Muscle environment showed a significant increase in permeability compared to bone environment. However, the extravasation rate was not significantly different from the control environment. This further indicates that vessel permeability was not the only factor contributing to extravasation. In Figure 7D, flow experiments were performed. Here, the interstitial shear was roughly 0.25 dynes/cm². These experiments are performed using the bone environment. Flow was observed to exert relevant effects on extravasation rate (decreased), permeability (decreased), and extravasation distance (increased). This showcases the significance of interstitial flow.

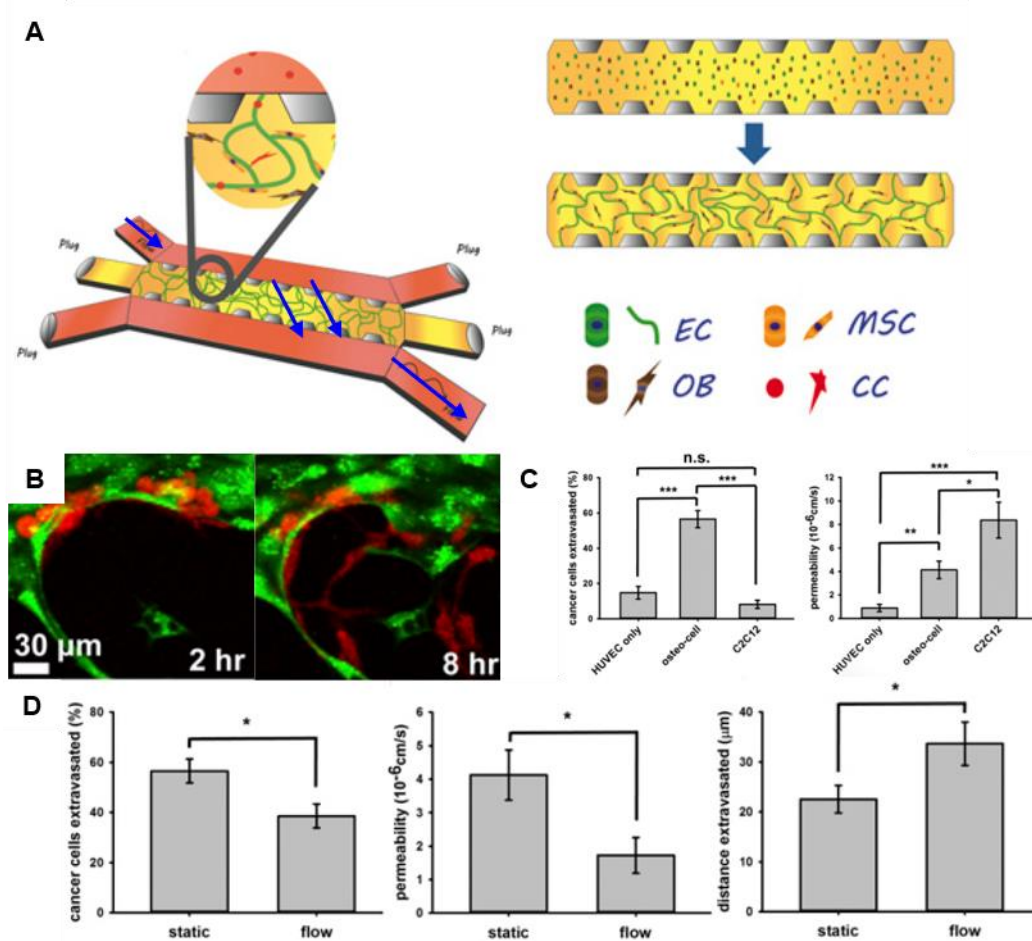


Figure 7: Bone organ-on-a-chip integrating interstitial flow. A: Schematic overview of the design. EC: Endothelial cells (HUVECs), MSC: Mesenchymal stem cells, OB: Osteoblasts, CC: C2C12 muscle cells. Blue arrows indicate the flow direction. B: Cancer cell (red) extravasation from vessel network (green). C: Quantification of cancer cell extravasation and vessel permeability in control, bone and muscle environment. D: Comparison of static and flow conditions for cancer cells in bone environment in terms of extravasation rate, vessel permeability, and extravasation distance. Adapted from [28].

1.4.3 Multi-organ-on-a-chips

Recently, multi-OoCs have been reported, aiming to mimic organ cross-talk instead of single organ functionality. The aim of these studies is to gain more insight into organ intercommunication. Not only cancer studies are of interest, but also other organ cross-talk studies have been reported. Some of the multi-OoC models reported are presented below.

Aleman et al. studied organ specificity using a tumor dissemination model. [29] In this design (Figure 8A+B), colon cancer tissue was cultured as well as endothelium, lung, and hepatic cells. These tissues were introduced in a hydrogel, and subsequently, the hydrogel was crosslinked using UV light. By perfusing medium from the colon spheroid towards the surrounding tissues, the tumor cells could enter the circulating medium flow and home to the surrounding tissues. Colon cancer cells were labeled so that homing can be examined. In Figure 8C+D it was presented that after 15 days of medium circulation colon cancer cells mostly home in lung tissue. Furthermore, cancer cells homed in the liver tissue. Cancer cells proved to home less in the endothelial compartment. This model could be promising for future drug testing and understanding of organ-specific cancer metastasis.

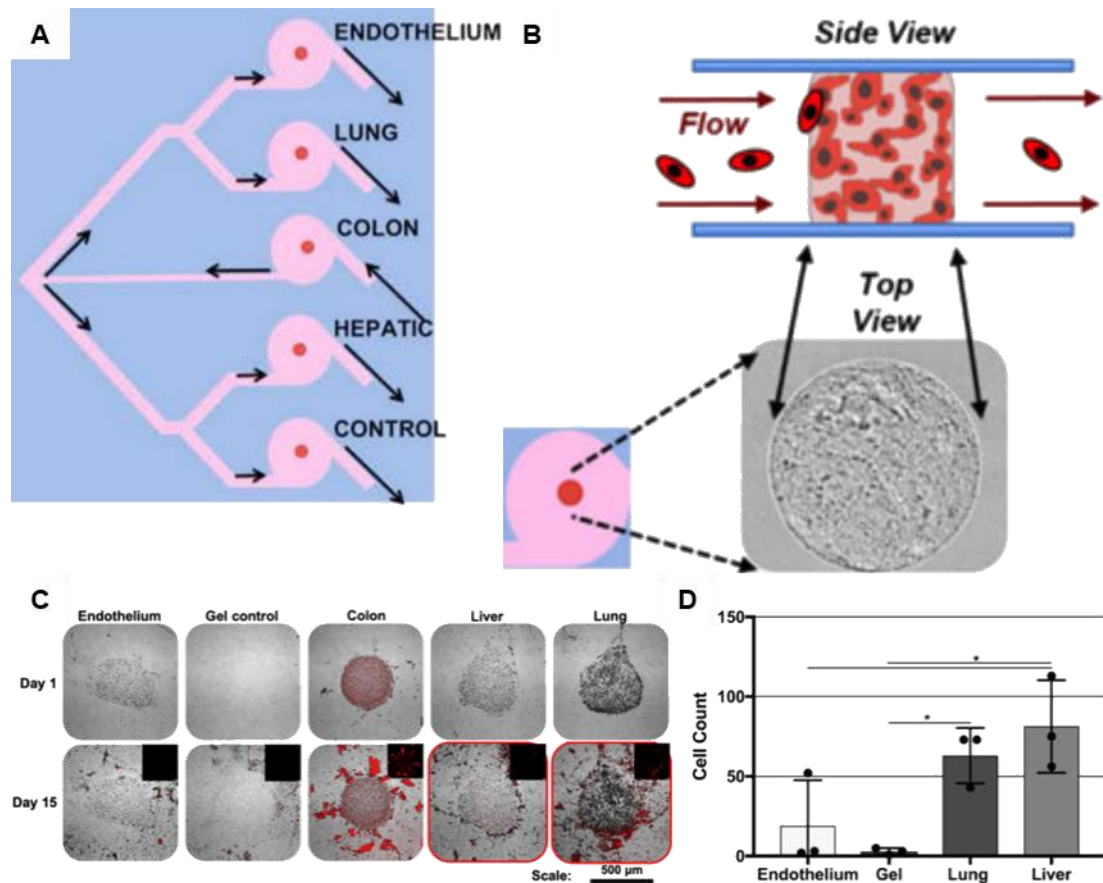


Figure 8: Overview of the multi-site metastasis-on-a-chip design. A: Schematic overview of the chip design. B: Schematic overview of the crosslinked hydrogel matrix inside the culture chamber. C: Microscopic images of tissues after 1 and 15 days. D: Tumor homing cell count upon 15 days (* $p < 0.05$). Adapted from [29].

In a metastasis-on-a-chip platform presented by Skardal et al., dissemination was established using one-way medium flow through two hyaluronic acid-based hydrogels containing colon cancer cells and healthy liver cells, connected in series. [30] The design and results were shown in Figure 9 below. Two different cancer cell types were cultured in the hydrogel. Cells were fluorescently labeled and imaged upon recirculation of medium. The more aggressive cell type (HCT116) disseminated to the downstream liver tissue, whereas a less aggressive cell type grew inside the primary gut, but did not intravasate. Upon culturing for >18 days, tumor extravasation was observed in the downstream liver tissue for the HCT116 cells.

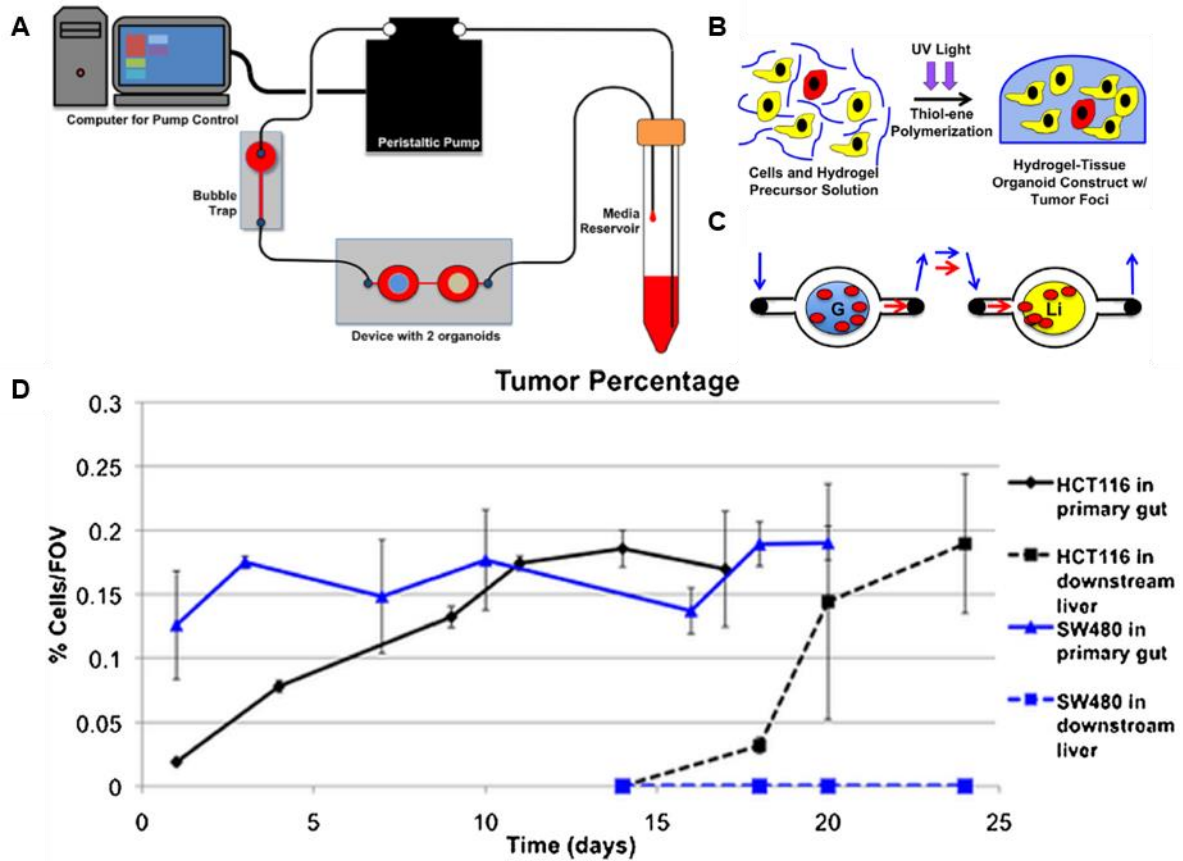


Figure 9: Overview of a metastasis-on-a-chip model. A: Schematic overview of the organ models connected in series to the circulation. B: Schematic of cell crosslinking in a hyaluronic acid-based hydrogel. C: representation of the flow direction from colon cancer to healthy liver. D: Tumor cell percentage in primary gut (solid lines) and downstream liver (dashed lines). The black lines represent data for a more aggressive cell type (HCT116), whereas the blue lines represent a less aggressive cell type (SW480). Upon 18 days, aggressive cancer cells homed into downstream liver tissue, whereas less aggressive cancer cells stayed in the primary tissue. Adapted from [30].

Lastly, another platform presented linked liver, lung, and heart modules in a single circulation. [31] The design and results were shown in Figure 10. The model aimed to recapitulate drug responses to predict unanticipated toxic by-effects. To this end, photo-crosslinked bio-inks containing organ specific cells were introduced in the circulation (Figure 10B). Upon introduction of bleomycin, an anti-cancer drug, initially no heart cytotoxicity was reported. However, in the presence of all organs, heart rate was hampered significantly (Figure 10C). It was shown that the lung module reacts to bleomycin by secreting IL-1 β (Figure 10D). This interleukin in effect caused hampering of cardiac organoid beating frequency (Figure 10E). The model proves to be effective in predicting multi-organ drug responses.

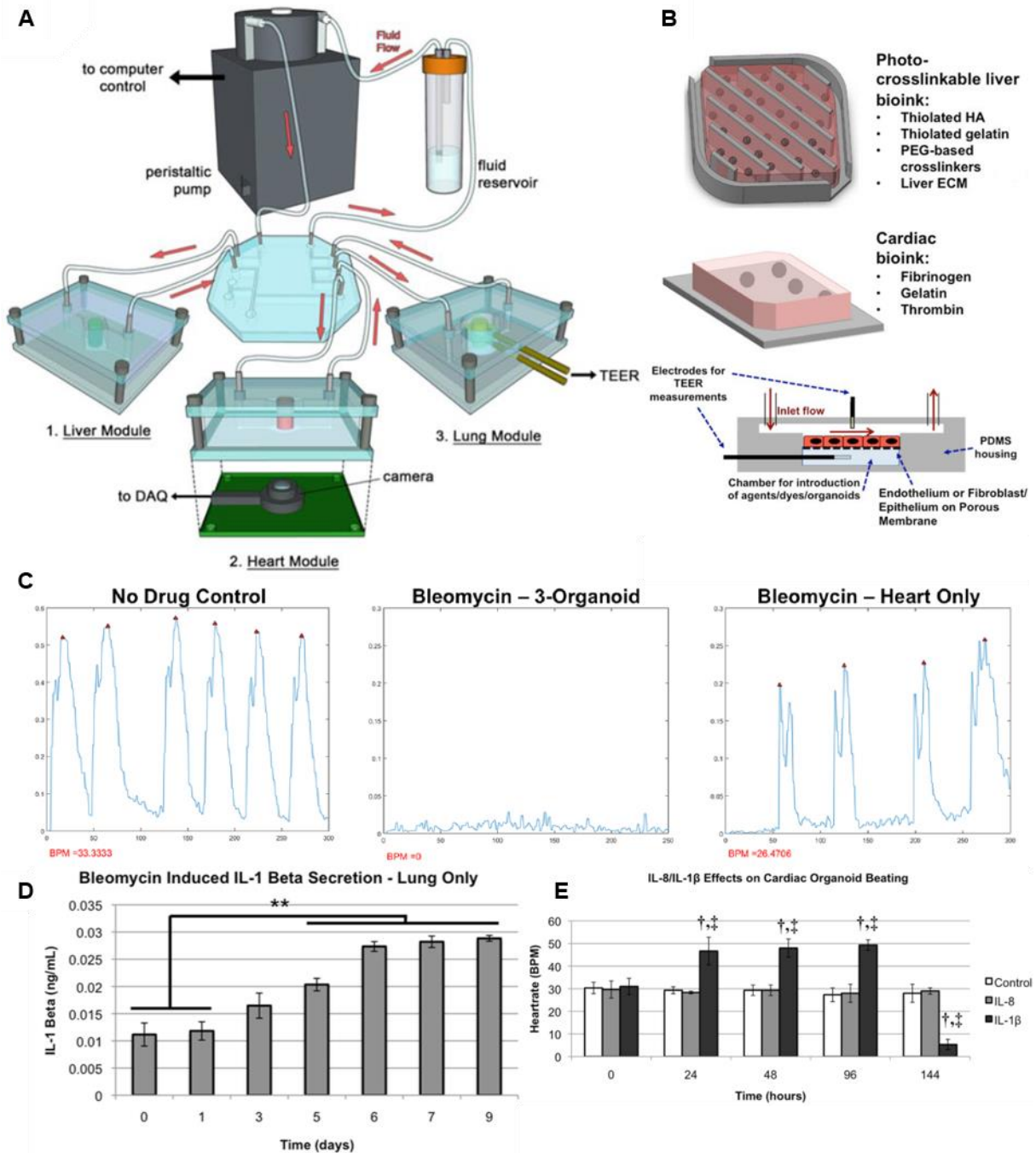


Figure 10: Overview of a multi-organ-on-a-chip platform comprising liver, lung, and heart tissue. Adapted from [31]. A: Overview of the circulation. B: Overview of the organs implemented in the circulation. C: Bleomycin affects cardiac organoid beating, only in the presence of all organs. D: Bleomycin induces IL-1 β secretion of the lung. E: IL-1 β significantly affects cardiac organoid beating frequency.

1.5 Remaining problem

All platforms presented before can contribute to a better understanding of parts of the metastatic cascade and can assist in the development and testing of therapeutics. What is still missing, however, is a system that allows cross-talk for 3D organ models of both tumor and target tissue in a single circulation, recapitulating all distinct steps of tumor metastasis (steps 1-5 shown in Figure 1). To correctly mimic the seed-and-soil principle, circulation has to be considered. First of all, as discussed before, only CTCs with very specific properties are capable to disseminate to the secondary organ. Furthermore, apart from biological effects, mechanical and geometrical effects related to blood circulation greatly affect the distribution of CTCs. Additionally, cells such as endothelial cells behave differently in the presence of flow. Proper shear stresses support endothelial cell quiescence and survival, vascular integrity and homeostasis. Shear stresses also change the endothelial cell morphology from cobblestone to spindle-like. Too low shear stresses stimulate inflammation, proliferation and apoptosis, destabilization of the barrier function, oxidative stress and dedifferentiation. [32] These cells are less responsive to various signals, such as signals that induce angiogenesis. [33] It is therefore of great importance to expose the endothelium to adequate shear stresses. Moreover, breast cancer cells exposed to interstitial flow (in bone environment) persist in a slow-proliferative state associated with increased drug resistance. [27] Both cross-talk and flow are thus of importance. Thirdly, in a circulation, kinetics and dynamics of cells and factors are more accurately mimicked, as it is possible that factors need to reach a certain threshold before exerting effects to the soil. By re-using the same medium multiple times, factors can increase concentration, eventually possibly affecting the OoCs integrated.

2 Aim & Requirements

2.1 Aim

The main aim of this thesis is to design a versatile and automated circulation that is compatible with OoC technology. The circulation should provide unidirectional flow and physiologically relevant shear stresses. Medium will be re-circulated to establish cross-talk between organs, whilst allowing factors and cytokines to increase in concentration over time. Sampling of the circulation will be on-demand for cellular and molecular analysis to eventually gain insight into the cross-organ communication processes. The circulation designed will not only be interesting for breast tumor dissemination, but will also pave the way towards examining essentially any condition comprising organ cross-talk.

2.2 Circulation requirements

In order to obtain a functioning circulation that is able to establish cross-talk between two organs, requirements have to be defined. The requirements of the circulation are listed below.

- **Versatility** The OoC models should be able to be connected to and disconnected from the circulation easily. This contributes to a decrease in failure rate, as a failed OoC can be replaced instantly. Moreover, it makes implementation of a wide variety of other organ models possible.
- **Organ cross-talk** In order to achieve organ cross-talk in a closed circulation, recirculation of medium has to be implemented. This way, molecular and cellular factors that possibly affect the primary and secondary microenvironment can gradually increase in concentration over time. This is a unique property of a closed loop circulation.
- **Unidirectional flow** In order to get a physiologically relevant endothelial barrier, the flow has to be unidirectional in the OoC at all times, so that endothelial cells can align to the flow. Alignment of endothelial cells to shear stresses is namely associated with higher responsiveness biological cues, continuous VE-cadherin network formation, actin stress fiber formation and realignment, and suppressed cell proliferation. These effects are not observed for bidirectional flow. [34]
- **Low internal volume** By keeping the volumes as low as possible, factors can possibly exert effects on the OoCs implemented in the circulation. Additionally, factors will not be diluted below the limit of detection. It is explained later (in section 6) how the amount of dilution of factors of interest will be determined and optimized. At the same time, a too low internal volume can lead to a depletion of nutrients, and eventually, cell death.
- **Sampling** A simple and effective sampling method has to be introduced in the system. Cytokines and circulating tumor cells (CTCs) are the main targets for analysis. For detection of cytokines using Enzyme-Linked Immunosorbent Assay (ELISA), 100 μL of sample is needed. [35] This means that either 100 μL could be sampled directly from the circulation, or a smaller volume could be sampled and diluted. The sampled volume can be replaced by fresh medium. This way, the experiment can continue upon sampling without losing significant amounts of factors present in the circulation. However, as CTCs are relatively rare, it is best to sample high amounts of medium to detect them. Therefore, it is best to sample for CTCs at the end of the experiment. Preferably, all volume will be sampled in this case.
- **Automation** The circulation has to be computer controlled, so that the circulation runs without assistance and parameters can be kept constant easily.
- **Physiological shear stress** Correct amount of shear has to be applied to achieve spindle-like endothelial cell morphology. Simultaneously, the flow has to provide nutrients. However, a too high flow rate can possibly cause damaging of the endothelial lineage.
- **Cell culture conditions** Cells and medium in the circulation have to be kept at 37°C and 5% CO₂. Additionally, a humidity of $\geq 80\%$ is recommended. All cells have to be nourished with a single medium source to allow use of a single closed loop circulation.

3 Materials & Methods

3.1 Organ-on-a-chip fabrication

3.1.1 Vessel-on-a-chip

Before fully established breast cancer and bone models will be integrated in the circulation, the blood circulation itself will be recapitulated. Therefore, the focus lies on implementing the endothelium first. An overview of the design of a vessel module is shown in Figure 11. A poly(dimethylsiloxane) (PDMS) chip consisting of $400\ \mu\text{m} \times 400\ \mu\text{m}$ channels of 1 cm long is produced (as well as a similar design with $600\ \mu\text{m} \times 600\ \mu\text{m}$ channels). This design was drawn using SolidWorks and printed using a 3D resin printer (Flashforge Hunter, FTD Black resin). The mold was washed once with acetone and ethanol, blow-dried, and cured for 15 min using 405 nm UV at an intensity of $14\ \text{mW}/\text{cm}^2$. Then, the mold was post-cured in an oven at 65°C for 24 h.

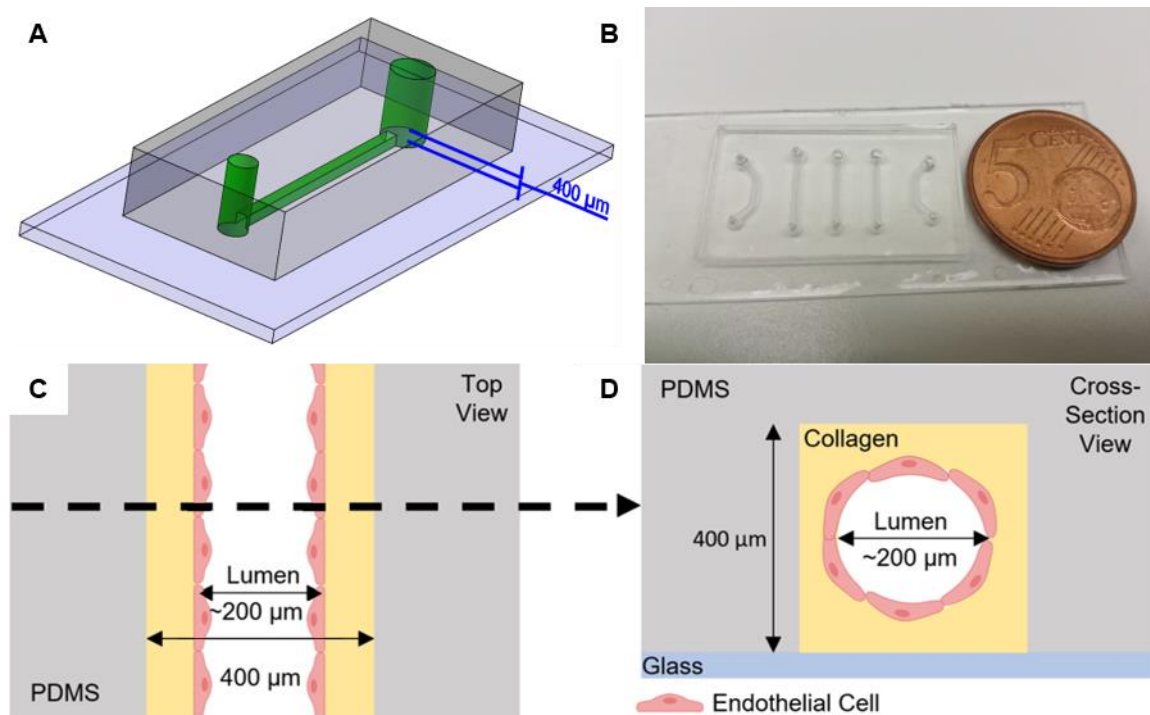


Figure 11: Overview of the vessel-on-a-chip used. A: SolidWorks drawing. B: Organ-on-a-chip bonded on a PDMS coated microscopy slide. C: Schematic top view of a Viscous Finger Patterned (VFP) lumen lined with HUVECs. D: Cross-sectional view of C. Cells illustrated using BioRender.

PDMS monomers were mixed with curing agent (Dow Corning) at a 10:1 weight ratio to obtain PDMS. Subsequently, PDMS was degassed. Then, PDMS was casted on the mold for 24 h after degassing. PDMS chips were removed from the mold and the inlet and outlet were punched at a diameter of 1 mm and 1.5 mm, respectively, using a biopsy puncher. Subsequently, OoCs were bonded to PDMS coated microscopy slides. PDMS coating of microscopy slides was performed by spin coating at 500 RPM for 5 sec and 1500 RPM for 30 s, and subsequent curing for 24 h. Then, OoCs were bonded after plasma treatment for 40 s at 50 W and 500 mTorr.

Chips were functionalized using 5 vol% (3-aminopropyl)triethoxysilane (APTES; Sigma-Aldrich) in milliQ water for 5 min, washed with ethanol and blow-dried. Then, 10 vol% glutaraldehyde (GA; Sigma-Aldrich) in PBS was incubated in the channel for another 5 min. Chips were rinsed with water followed by ethanol and blow-dried after GA treatment. Then, chips were cured in an oven at 65°C for at least 3 h. Viscous Finger Patterning (VFP) was then performed using collagen type I (Corning) at a concentration of 5 mg/mL (Figure 12). [36] 1M NaOH was used to keep the pH of the collagen mixture between 7.4 and 8.0. After introduction of collagen to the channel, a droplet of ~20 μ L medium was added to the outlet of the channel. Then, by pipetting small ~2 μ L droplets of medium on the inlet, a flow is established between inlet and outlet. Due to Laplace forces and differences in viscosity, the small droplet sucks through the channel towards the outlet, leaving a cylindrical lumen in the process. Patterned chips were incubated for 30 min at 37°C to crosslink the collagen and stored for at least 3 h at 4°C in PBS or at 37°C in medium to make sure pH equilibrates.

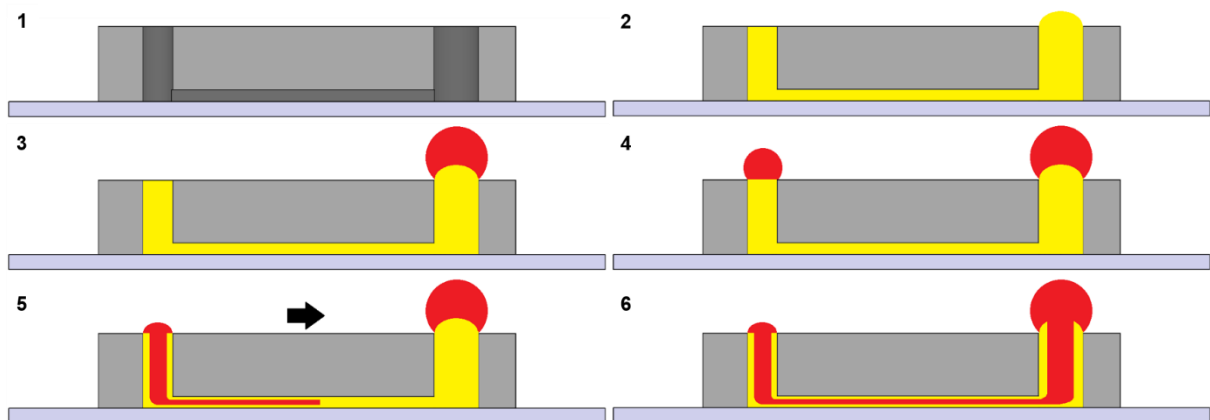


Figure 12: Overview of the Viscous Finger Patterning (VFP) technique. 1: Cross-sectional side view of a straight channel 2: Collagen (yellow) is introduced in the channel after APTES/GA treatment. 3: A large droplet of medium (red) (~20 μ L) is placed on top of the outlet (1.5 mm diameter). 4: Small droplets of medium (~2 μ L) are sequentially pipetted on the inlet (1 mm diameter). 5: Due to Laplace forces and difference in viscosity, a flow is created as depicted by the arrow, leaving a cylindrical lumen in the process. 6: Fully formed microfluidic channel.

3.1.2 Breast tumor-on-a-chip

Apart from a vessel module only, OoCs designed to mimic the target organ have to be implemented in the circulation. In Figure 13, a breast tumor-OoC design is proposed.

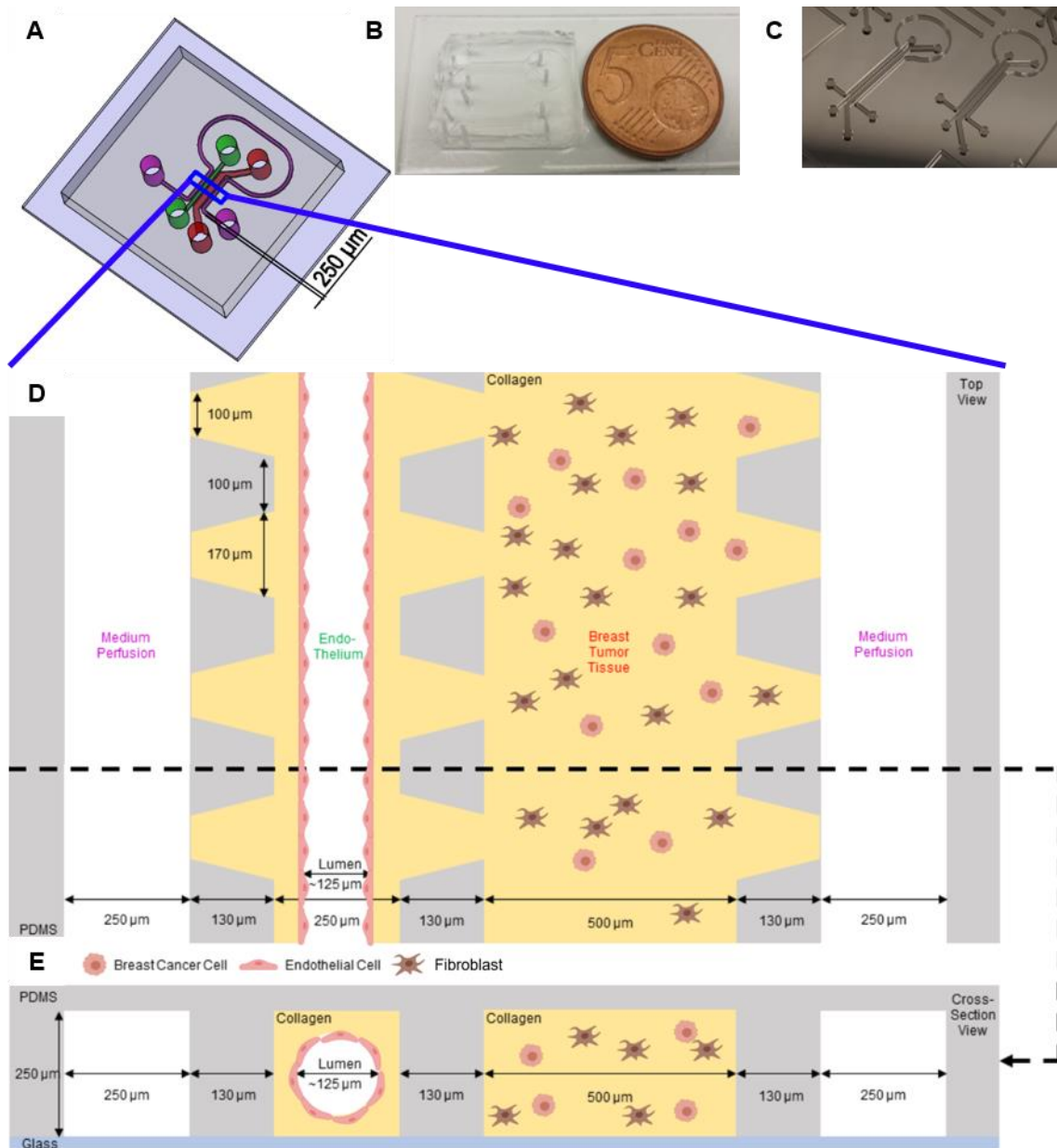


Figure 13: Overview of the breast tumor-on-a-chip design. A: SolidWorks drawing. Note that medium perfusion in the side channel (pink) is performed using a single channel. B: Organ-on-a-chip device bonded on a PDMS coated microscopy slide. C: Photo of the mold fabricated using an SU8 wafer. D: Schematic top view of the OoC after VFP and introduction of all cell types. E: Cross-sectional view of D. Cells illustrated using BioRender.

The design combines the vessel part that was presented and studied earlier with an additional channel where cells can be cultured in 3D environment in collagen, separated by pillars. This way, breast tumor tissue can directly communicate with the integrated vessel. By culturing cancer cells as well as fibroblasts in the OoC, breast tumor microenvironment can be recapitulated.

As the pillars have a high aspect ratio and small size, the production of this device can not be produced using the 3D printer. Therefore, this mold is produced using soft-lithography in the cleanroom. [37] Cleanroom steps were performed by Carlo A. Paggi. Using Clewin5 software (WieWeb software, Netherlands) the design was drawn. A quartz mask corresponding to this design was generated by etching a chromium layer after direct-writing using a high-resolution laser. The quartz mask was used for photolithography using SU-8 on a silicon wafer, to produce a mold. Briefly, a ~250 μm layer of SU-8 photoresist was spin-coated on the surface of a silicon wafer. The quartz mask was next placed on the surface of the wafer and a beam of UV light was used to photo-polymerize the photoresist not covered by the design present on the mask. The wafer was subsequently washed to remove the uncured photoresist and subjected to a post-bake.

Further fabrication of OoCs was identical to the protocol described in section 3.1.1. An additional post-treatment step was performed in the oven for 24 h after plasma bonding to reduce hydrophilicity. [38] This increases the collagen retention capacity of the pillars.

3.2 Cell culture & seeding

Human Umbilical Vein Endothelial Cells (HUVECs) were cultured using EGM-2 medium (PromoCell) and used for seeding exclusively between passages 3-8. Human Mammary Fibroblasts (HMFs) were cultured using Fibroblast medium (FM) supplemented with 10% FBS, 1% fibroblast growth supplement, and 1% P/S (ScienCell). HMFs were used exclusively between passages 3-15. MDA-MB-231 cells were cultured using Dulbecco's Modified Eagle Medium (DMEM) supplemented with 10% FBS, 1% P/S and 1% Gmax (GIBCO). MDA-MB-231 cells were chosen as breast cancer cell line due to the highly invasive behavior of this cell type. [39] Human Mammary Endothelial Cells (HMECs) were cultured using EGM-2 medium (PromoCell). HMECs were used exclusively between passages 3-8. All cell types were cultured in T75 flasks in a standard cell incubator.

For seeding, HUVECs were washed once with PBS, trypsinized using 0.25% trypsin-EDTA (GIBCO) for 3 min at 37°C and centrifuged at 300 G for 3-5 min. HMECs were washed with Dulbecco's PBS. HUVECs and HMECs were seeded at final a cell concentration varying from 4-10 cells/mL. 10 μL of cell suspension was used to seed per channel. Typically, cells seeded at a higher density (10 million cells/mL) were used after 24 h, whereas cells seeded at a lower density (4 million cells/mL) were used after 72 h. HMECs were seeded at 4 million cells/mL and used after 24 h. 1 h after the first seeding, channels were washed with fresh medium, and a second seeding was performed. OoCs were flipped upside down so that cells could adhere to the top of the channels. Channels were provided with fresh medium daily. This was done by introducing new medium via the inlet, and removing the old medium using an aspiration system.

3.3 HEPES buffer concentration optimization

In standard cell culture conditions, CO₂ regulates pH through the bicarbonate buffering system. In general, physiological pH is considered to be in the range of 7.2 to 7.4. However, some disease states such as cancer may require a lowered pH. [40] To control pH in a CO₂ lacking environment, N-2-hydroxyethylpiperazine-N'-2-ethanesulfonic acid (HEPES) can be supplemented to culture medium. HEPES is a zwitterionic buffer with a pKa of 7.3 at 37°C that is commonly used to buffer cell cultures. [41]

Before usage of HEPES in cell culture experiments, the best suiting concentration of HEPES was determined in terms of cytotoxicity and buffering efficacy. All HEPES concentration assays were performed using 2D culture well plates. After 94 h of culturing with HEPES conditions, a PrestoBlue assay (Thermo Fisher) was performed to determine the metabolic activity of the cells. Furthermore, a Blue/Green cell viability assay (Thermo Fisher) was performed on the same sample. The Blue/Green viability staining was used following manufacturers' protocol. 200 µL was added per well and incubated in a dark environment for 30 min at RT. Then, samples were imaged using fluorescent microscopy. PrestoBlue assays were performed following manufacturers' protocol. 200 µL was added per well and incubated in a dark environment for 30 min at RT. Then, a fluorescent readout was performed using a plate reader. Excitation was set at 540-570 nm and emission at 580-610 nm.

3.3.1 HUVECs

HUVECs were cultured in a 48-well plate for 72 h at a seeding density of 20,000 cells/well under standard culture conditions. Then, HEPES buffered medium was added at concentrations of 0 (control), 10, 25, and 100 mM for 96 h and cultured in the Ibidi stage-top incubator. Medium was refreshed once after 48 h.

3.3.2 HMECs, HMFs, MDA-MB-231

HMECs, HMFs and MDA-MB-231 cells were seeded at 10,000 cells/well in a 96-well plate and cultured for 48 h under standard culture conditions. Then, HEPES buffered cell medium was added at concentrations of 0 (control), 10, 25, and 100 mM. Cells were cultured under HEPES conditions for 94 h in an Ibidi stage-top incubator. after 24 h, medium was refreshed once.

3.3.3 Co-Culture of HMF:MDA-MD-231

HMFs and MDA-MB-231 cells were co-cultured at a final seeding density of 10,000 cells/well in a 96-well plate. Ratios used were HMF:MDA-MB-231 1:1, 2:1, 3:1, and 4:1. Cells were cultured for 48 h under standard culture conditions, using FM:DMEM medium mixed in ratios corresponding to the cell seeding ratios. Then, HEPES buffered medium was mixed in the same medium compositions and added at concentrations of 0 (control), 10, and 100 mM. Cells were cultured under HEPES conditions for 94 h in an Ibidi stage-top incubator. Medium was refreshed once after 72 h.

An MFCS-EZ pressure pump with a 0-2000 mbar range (Fluigent), Flow Unit size M (Fluigent), Switch Board (Fluigent), Flow Board/Flow Rate Platform (Fluigent), and L-switch (Fluigent) were connected using tubing with an Inner Diameter (ID) of 0.02 IN and an Outer Diameter (OD) of 0.06 IN (Tygon). The pressure controller was connected to the flow rate platform. The pressure controller was supplied with constant N₂ source using a pressure valve. The pressure controller was in turn connected to 2 mL Eppendorf reservoirs. OoCs were connected using flexible tubing (Tygon), making it easy to connect and disconnect different parts in the system.

The switchboard, flow rate platform, and pressure controller were connected to a laptop. Fluigent All-in-one, Microfluidic Automation Tool (MAT), and ESS control software was used to control the circulation. All-in-one software was used to control the pressure pump and monitor output of the flow unit, whereas ESS control was used to control the switchboard and thus the L-switch. Using an L-switch, capable to rotate in 2 distinct positions, recirculation of medium was mimicked (Supplementary Figure 1). The L-switch can change flow direction inside the reservoirs, while keeping the flow inside the OoCs unidirectional. By regularly altering the L-switch position at given time points, a recirculating motion can be mimicked. Flow can be controlled using a flow meter.

3.4.2 Cell culture conditions

As mentioned before, it is important that cell culture conditions can be established using the circulation. A well plate sized stage-top incubator (Ibidi) was implemented in the circulation, consisting of a gas mixer, heating system, and humidifying column to provide culture conditions similar to those in a conventional incubator (Figure 4B+D). The incubator can keep the medium and cells at 37°C, >75% humidity and 20-21% O₂. As no pressurized CO₂-source is available in the lab, HEPES was used to supplement the medium, so that the medium is CO₂ independent. Buffering of medium using HEPES was optimized first. This is described before in section 3.2.

3.4.3 Automation

Microfluidic Automation Tool (MAT, Fluigent) can be used to design and operate a circulation protocol. Two pressure channels connected to reservoirs and an L-switch should be controlled automatically to obtain circulation and thus cross-talk between organs. An automation protocol is presented below in Figure 15.

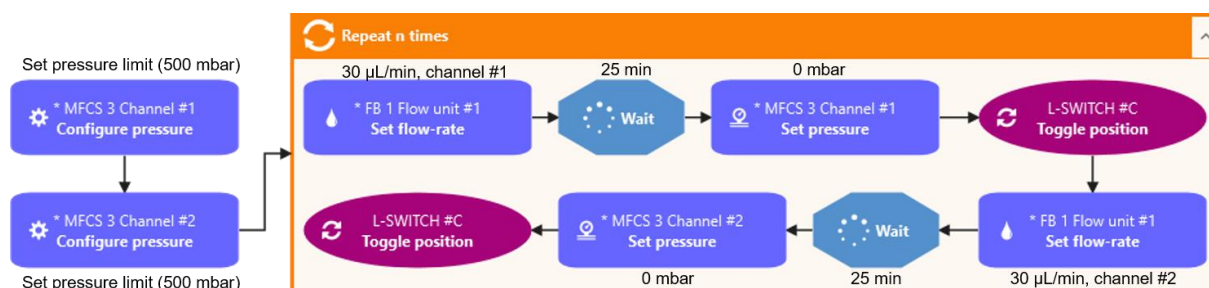


Figure 15: Overview of the protocol designed in the Microfluidic Automation Tool by Fluigent. First, a pressure limit is set for the input pressure channels, so that the system cannot damage the cells if the feedback loop fails. Then, a repeating loop will be initiated. First, the flow rate will be set at 30 µL/min using pressure channel #1. After 25 minutes, the pressure will be set at 0 mbar, the L-switch toggles position and the flow rate will be set at 30 µL/min using pressure channel #2. Finally, the pressure of channel #2 will be set at 0 mbar, the L-switch toggles to its initial position and the loop restarts with setting the flow rate at 30 µL/min using pressure channel #1. The amount of repeats can be set at a high value, as the circulation will be paused or stopped manually when sampling is performed. Each loop, 750 µL is displaced per reservoir.

3.4.4 Flow output

Characterization of flow output was performed using MAT. ~1 day (21.5 h) of data was used to determine the stability of the flow output. A measurement was performed by the software roughly each 54 ms (meaning that roughly 1.4 million data points were collected).

3.5 Providing shear conditions

As discussed before, HUVECs need adequate shear stresses to establish behavioral as well as morphological changes. In literature, shear stresses reported for HUVECs in microfluidic channels vary between 1-16 dynes/cm². [33, 42, 43] DeStefano *et al.* [33] assessed multiple shear stresses in fibronectin coated microfluidic channels containing HUVECs. They concluded that shear stresses ranging from 4-16 dynes/cm² are sufficient to transition cells from a cobblestone to a spindle-like morphology. Shear stresses of 8, 12, and 16 dynes/cm² showed to increase proliferation and decrease cellular apoptosis compared to 4 dynes/cm². This is in accordance with other studies conducted: shear stresses ≥ 5 dynes/cm² are sufficient to change morphology and proliferation rate of the HUVECs. [42, 43]

The theoretical flow needed to obtain a shear of 5 dynes/cm² can be calculated using:

$$\tau = \frac{4Q\mu}{\pi r^3}, \text{ and its rewritten form } Q = \frac{\tau\pi r^3}{4\mu} \text{ [44]}$$

where τ is the shear rate in Pa, Q is the flow rate in m³/s, r is the radius of the lumen in m and μ is the dynamic viscosity (for EGM-2, the dynamic viscosity is $7.8 \cdot 10^{-4}$ Pa·s at 37°C). [34] The first design consisted of channel dimensions of 600 μ m x 600 μ m, resulting in lumen diameters expected to be around 400 μ m. [36]

After optimization, another vessel module with channel dimensions of 400 μ m x 400 μ m was designed, so that the lumen diameter is expected to be around 200 μ m upon VFP. [36] To obtain a shear stress of 5 dynes/cm² or 0.5 Pa, the desired flow rate for these 200 μ m lumens is therefore ~ 30 μ L/min.

3.5.1 Syringe pump

Before Implementation of the vessel models in the circulation platform, the models are studied using a simple syringe setup (Figure 16). Cells are seeded at an expected density of 10 million cells/mL as presented in section 3.2, and cultured for 24 h before flow application. Flow is applied for 24 h, as shear application for ≥ 16 h is sufficient to change the morphology of the HUVECs to spindle-like cells. [44] Instead of a pushing motion, the syringe pump withdraws medium. Increasing the pressure by pushing in the syringe can namely cause spontaneous gas formation. [45]

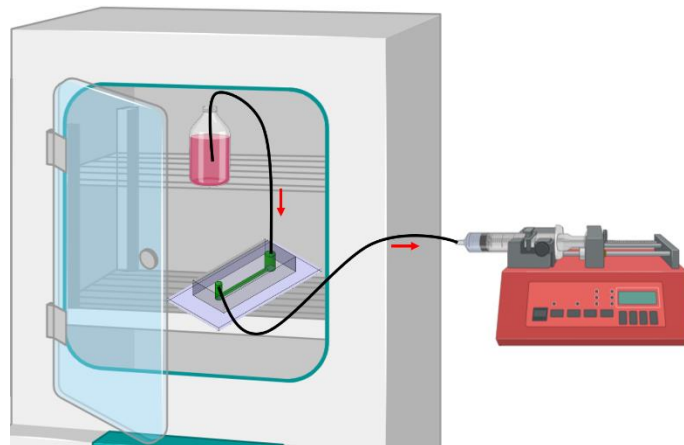


Figure 16: Schematic overview of the experimental setup used to assess the effect of shear on Human Umbilical Vein Endothelial Cells (HUVECs). Created using BioRender

3.5.2 Circulation setup

After optimizing the shear stress using the syringe setup shown in the figure above, HUVEC morphology and viability was characterized after flow application for 24 h using the circulation. EGM-2 medium was supplemented with 10 mM HEPES. HMECs were tested using the same conditions afterwards.

Following flow application, a viability assay was performed to check viability as well as cell morphology. To this end, Calcein AM and Ethidium Homodimer-1 (Thermo Fisher) were diluted to final concentrations of 4 μM and 2 μM , respectively. 10 μL per channel was introduced and incubated in dark environment for 30 min at RT. Viability can be qualitatively assessed using live/dead staining, and using ImageJ (FIJI), the directionality distribution of the HUVECs was assessed using only the live channel of the image.

3.6 Breast tumor-on-a-chip characterization

Breast tumor-on-a-chip designs were characterized based on feasibility to perform VFP in the decreased channel size and feasibility to introduce cells. To this end, VFP was performed, and subsequently, MDA-MB-231 cells were introduced stained with green CMFDA CellTracker (Thermo Fisher). To this end, cells were incubated first for 30 min under normal culture conditions using 20 μM CellTracker in FBS free medium. Cells were seeded at a concentration of 10 million cells/mL in the endothelial channel. Then, for the hydrogel channel, cells were mixed 1:1 with collagen to obtain a final collagen concentration of 4.5 mg/mL and a cell seeding density of 5 million cells/mL.

3.7 Imaging

Imaging was performed using an EVOS M5000 microscope (Thermo Fisher). Filters used were: DAPI (Ex: 357/44 nm, Em: 447/60 nm), GFP (Ex: 470/22 nm, Em: 525/50 nm), and RFP (Ex: 531/40 nm, Em: 593/40 nm).

3.8 Statistics

Statistical significance was analyzed using one-way ANOVA & Post-Hoc Tukey's test in Origin (OriginLab). Population mean μ and standard deviation σ were calculated using the equation shown below in Microsoft Excel:

$$\mu = \frac{\sum X}{N}, \sigma = \sqrt{\frac{\sum (X - \mu)^2}{N}}$$

3.9 Image processing

Figures were made using Microsoft PowerPoint, BioRender, and SolidWorks. Graphs were generated using OriginLab. EVOS images were processed using ImageJ.

4 Results & Discussion

In this section, a circulation is presented that is compatible with multiple OoCs. First, HEPES buffering capacity as well as cytotoxicity is examined, as HEPES is needed to account for the lack of CO₂ in the culture environment of the Ibidi stage-top incubator. Then, the circulation is described. The focus lies on flow output stability, internal volume, and sampling methods. Subsequently, results are presented with respect to providing physiological shear conditions to endothelium. This is first established using a syringe pump setup, and later using the circulation. HUVECs are the main cell type characterized, but preliminary results for HMECs are presented as well. Lastly, future breast tumor-on-chip designs are proposed and discussed.

4.1 HEPES buffer concentration optimization

The Ibidi stage-top incubator provides cells with 20-21% O₂, >75% humidity and a temperature of 37°C. However, as no CO₂ source was available in the laboratory, cell medium was supplemented with HEPES to obtain CO₂-independent medium. Therefore, in this subsection, HEPES concentration is optimized. Cytotoxic effects of HEPES have already been reported extensively. It has been reported that increasing concentrations of HEPES progressively increase nitroblue tetrazolium reduction, indicating higher formation of O₂⁻, a compound known to rapidly form toxic byproducts. Furthermore it has been reported that HUVEC growth retarded at 25 mM HEPES buffer concentration. [46] Moreover, growth of human cancer cells is promoted by the presence of a standard 5% CO₂ environment, and therefore it is beneficial to mimic this environment *in vitro*. [47] Thirdly, it has been reported that HEPES causes generation of phototoxic compounds when exposed to visible light in medium. [48] This all leads up to the fact that HEPES should be used with caution in all cases.

4.1.1 Human Umbilical Vein Endothelial Cells

The results of HUVECs cultured with various concentrations of HEPES are shown below in Figure 17.

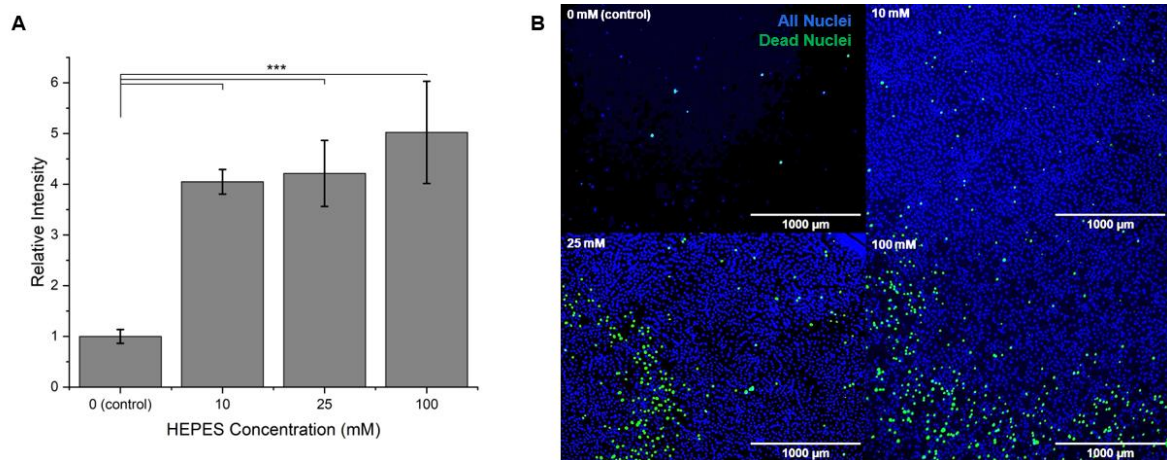


Figure 17: HUVECs with various HEPES buffer concentrations. A: PrestoBlue assay results. *** indicates $p < 0.005$. B: Overview of ReadyProbes Blue/Green cell viability assay. Blue dots indicate cell nuclei, whereas green dots indicate nuclei of dead cells.

It immediately becomes clear that CO₂-independent medium is needed, as cells in the non-buffer containing control died and flushed out of the well plates. Figure 17A proves that 10, 25, and 100 mM are all suitable concentrations as the metabolic activity was significantly ($p < 0.005$) increased compared to the control. However, Figure 17B shows that concentrations of 25 and 100 mM cause an increase in cell death. Therefore, a HEPES concentration of 10 mM is used in further experiments. The metabolic activity of cells cultured in 100 mM HEPES buffered medium was slightly larger compared to 10 mM and 25 mM HEPES conditions. This could imply that cells under extreme culture conditions react to the environment with increased metabolic activity before dying. All in all, 10 mM of HEPES is used in further experiments as it provides adequate buffering without retarding cell growth.

4.1.2 Human Mammary Endothelial Cells

As multiple cell types were used in future OoC designs to mimic the breast microenvironment, the optimal HEPES concentration has to be determined for these cell types as well. Firstly, results for HMECs are presented in Figure 18.

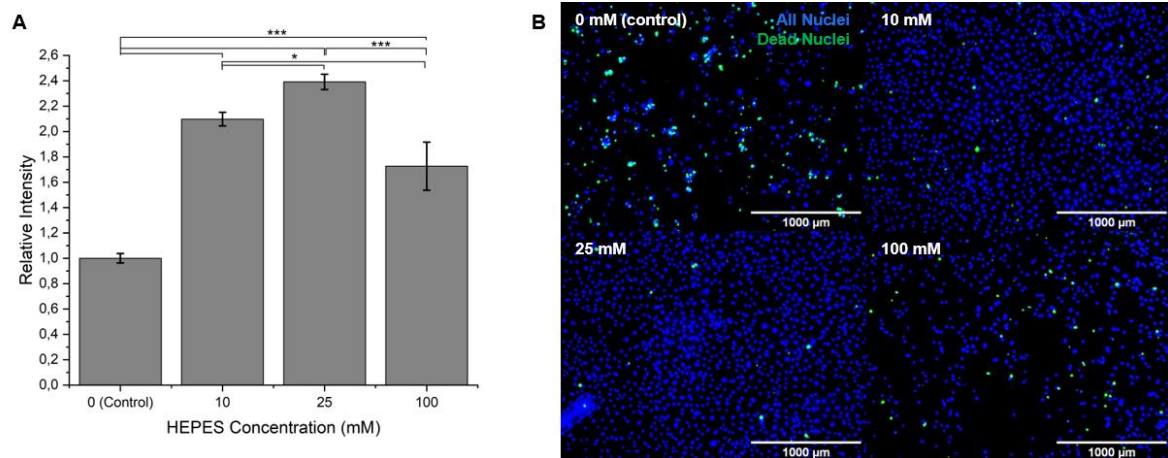


Figure 18: HMECs with various HEPES buffer concentrations. A: PrestoBlue assay results. * indicates $p < 0.05$, *** indicates $p < 0.005$. B: Overview of ReadyProbes Blue/Green cell viability assay. Blue dots indicate cell nuclei, whereas green dots indicate nuclei of dead cells.

The results are similar to those for HUVECs: a concentration of 10 mM does not seem to alter viability and growth of cells, whereas 0 mM and 100 mM of HEPES significantly affects viability. Therefore, 10 mM was determined to be a suitable concentration.

4.1.3 Human Mammary Fibroblasts

In Figure 19, the results corresponding to HMFs cultured in varying HEPES conditions are presented.

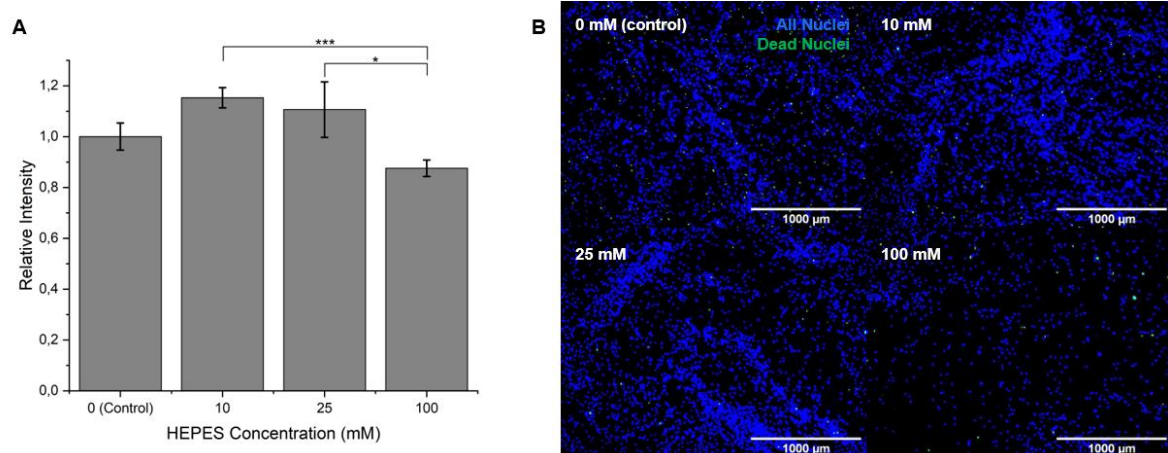


Figure 19: HMFs with various HEPES buffer concentrations. A: PrestoBlue assay results. * indicates $p < 0.05$, *** indicates $p < 0.005$. B: Overview of ReadyProbes Blue/Green cell viability assay. Blue dots indicate cell nuclei, whereas green dots indicate nuclei of dead cells.

Interestingly, HMFs seem to grow independently of the CO₂ amount, as the control sample shows great viability as well as metabolic activity. This could be explained by the fact that fibroblasts are known to endure pH changes down to 6.5. [49] At 100 mM HEPES, viability is decreased. Again, 10 mM seems to be a suitable HEPES concentration.

4.1.4 MDA-MB-231 Cells

Figure 20 presents the data obtained for MDA-MB-231 cultured in HEPES conditions.

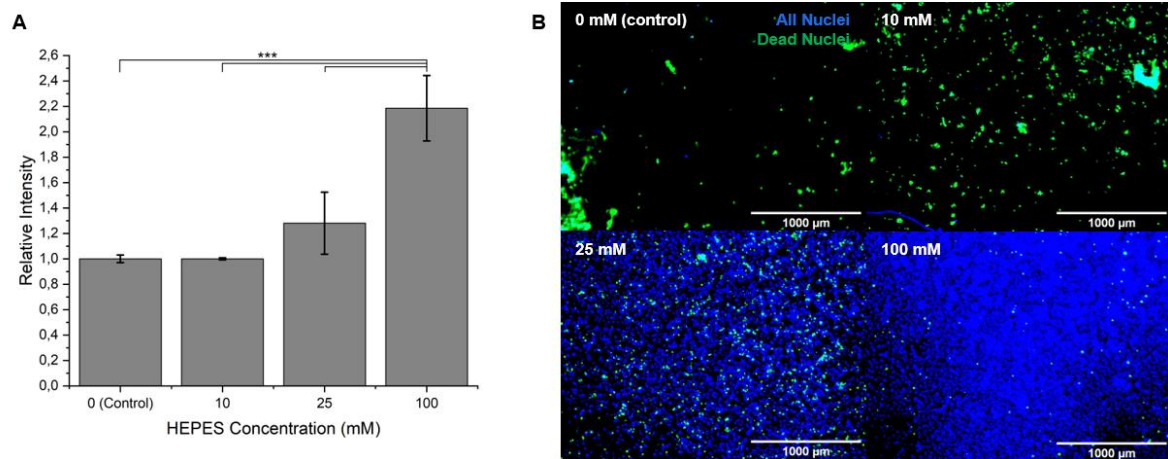


Figure 20: MDA-MB-231 Cells with various HEPES buffer concentrations. A: PrestoBlue assay results. *** indicates $p < 0.005$. B: Overview of ReadyProbes Blue/Green cell viability assay. Blue dots indicate cell nuclei, whereas green dots indicate nuclei of dead cells.

MDA-MB-231 cells behaved differently in presence of HEPES compared to the previous shown cell types. MDA-MB-231 cells seemed to grow better in high buffer concentration conditions. This could very well be due to the high turnover rate of this cell type.

4.1.5 Co-Culture of Human Mammary Fibroblasts & Human Breast Cancer Cells

In the breast cancer microenvironment, breast cancer cells co-exist with other cell types, fibroblasts being the most abundant. Therefore, *in vitro* models often co-culture cancer cells along with fibroblasts. Co-cultures of breast cancer cells to cancer associated fibroblasts are reported in literature at widely varying ratios. Co-culture experiments report ratios ranging from 1:0.25 to 1:5 in 2D as well as 3D and microfluidic culture approaches. [12, 50–53]

The results of a co-culture experiment performed using ratios of HMF:MDA-MB-231 1:1, 2:1, 3:1, and 4:1 are presented in Figure 21.

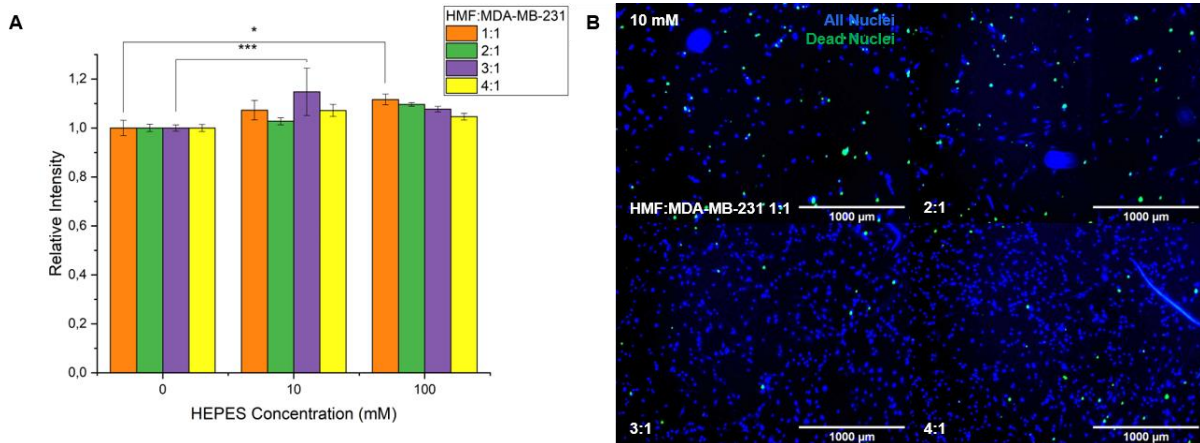


Figure 21: HMF & MDA-MB-231 co-culture at varying ratios with varying concentrations of HEPES. A: PrestoBlue assay results for different ratios of HMF:MDA-MB-231. * indicates $p < 0.05$, *** indicates $p < 0.005$. B: Overview of ReadyProbes Blue/Green cell viability assay. Blue dots indicate cell nuclei, whereas green dots indicate nuclei of dead cells.

From the live/dead results, it has been shown that at a higher ratio of HMFs ($\geq 3:1$), the cells seem to show higher viability, as there is an increased cell count. The confluency of cells (estimated based on transmitted light images) is 10-15% for cells cultured at 1:1 and 2:1 ratios, whereas the confluency of cells cultured at 3:1 and 4:1 ratios was ~30%. However, the PrestoBlue assay is less conclusive. There seems to be a trend that shows that for increasing HMF ratio, 10 mM buffering is more suitable. For a ratio of $\leq 2:1$ HMF:MDA, it seems that 100 mM HEPES still works best (live/dead results not shown). These observations can however not be concluded from the graph as there are no significant changes detected. From the live/dead results, it seems to become clear that at an increased HMF ratio ($\geq 3:1$), the buffering capacity of HEPES at a concentration of 10 mM is increased, without decreasing the cell viability significantly. Ratios $< 3:1$ are not recommended to use along with HEPES buffering, as it might cause significant growth retarding. To prevent cell death, the initial seeding density of MDA-MB-231 cells has to be low compared to the concentration of HMF cells. The ratio of HMF:MDA-MB-231 will however be determined based on the ability to mimic *in vivo* environment, and therefore an alternative for HEPES has to be introduced if the buffering capacity of HEPES is not adequate at 10 mM.

It has to be noted that proliferation and metabolic activity cannot be extrapolated easily to a 3D culture environment, especially in terms of metabolic activity. [54] Additionally, culture in a 2D well plate is significantly different than culture in a PDMS microdevice. Therefore, 3D culture experiments using the OoC design have to be performed in order to be conclusive on HEPES concentration optimization.

Additionally, it is important to note that no control was included of cells cultured in standard culture conditions at 5% CO_2 without HEPES buffering. In further experiments, it is important to include this positive control.

4.2 Circulation optimization

4.2.1 Flow output stability

The circulation was optimized in terms of flow stability without implementation of OoC models. First, the circulation showed a flow rate that was fluctuating occasionally between 20 and 40 $\mu\text{L}/\text{min}$ (Supplementary Figure 2). This could be explained by the fact that the fluidic resistance was too low. The pressure provided by the pump was between 0-50 mbar, whereas the pump is capable to provide pressures ranging up to 2000 mbar. The input pressure was so small even that the steps were corresponding to the resolution of the pump (steps of 0.63 mbar). Therefore, it was hard to obtain stable flow. Microfluidic resistance was therefore increased using a ~ 15 cm piece of 127 ID tubing (PEEK).

In Figure 22, representative output of the Fluigent setup upon increasing the microfluidic resistance is presented. The results were generated without implementation of OoC models. The mean flow is determined to be $29.92 \pm 2.29 \mu\text{L}/\text{min}$. Flow was stable within seconds upon switching of the L-switch. The minimum flow rate detected was $-120 \mu\text{L}/\text{min}$, which corresponds to the highest negative flow the flow unit can measure. This flow rate was observed for a very short time period (1 data point, thus ~ 54 ms) upon switching of the circulation. However, as the actual flow rate is unknown and could very well be greater than $120 \mu\text{L}/\text{min}$, it is possible that cells are affected by this sudden change in flow rate. It is however more likely that it is an artifact in the feedback loop due to the brief switch time needed for both L-switch and pressure input channel. The maximum flow rate detected was $71.5 \mu\text{L}/\text{min}$. A flow rate of $50\text{-}72 \mu\text{L}/\text{min}$ was observed in the first 2 minutes upon switching during this period. A flow of $72 \mu\text{L}/\text{min}$ corresponds to a shear of roughly $12 \text{ dynes}/\text{cm}^2$, and is thus unlikely to damage the cells. A brief drop in flow (just below $20 \mu\text{L}/\text{min}$ for 9 min) followed by an increase in flow ($>40 \mu\text{L}/\text{min}$ for 1.5 min) was observed. This is also not expected to significantly affect the cells. Overall, despite some fluctuations, the circulation provides stable and easily controllable flow with a stable mean flow rate ($29.92 \mu\text{L}/\text{min}$), and outliers ($-120 \mu\text{L}/\text{min}$ to $71.2 \mu\text{L}/\text{min}$) that are not expected to cause significant behavioral changes of the cells in the ongoing experiment.

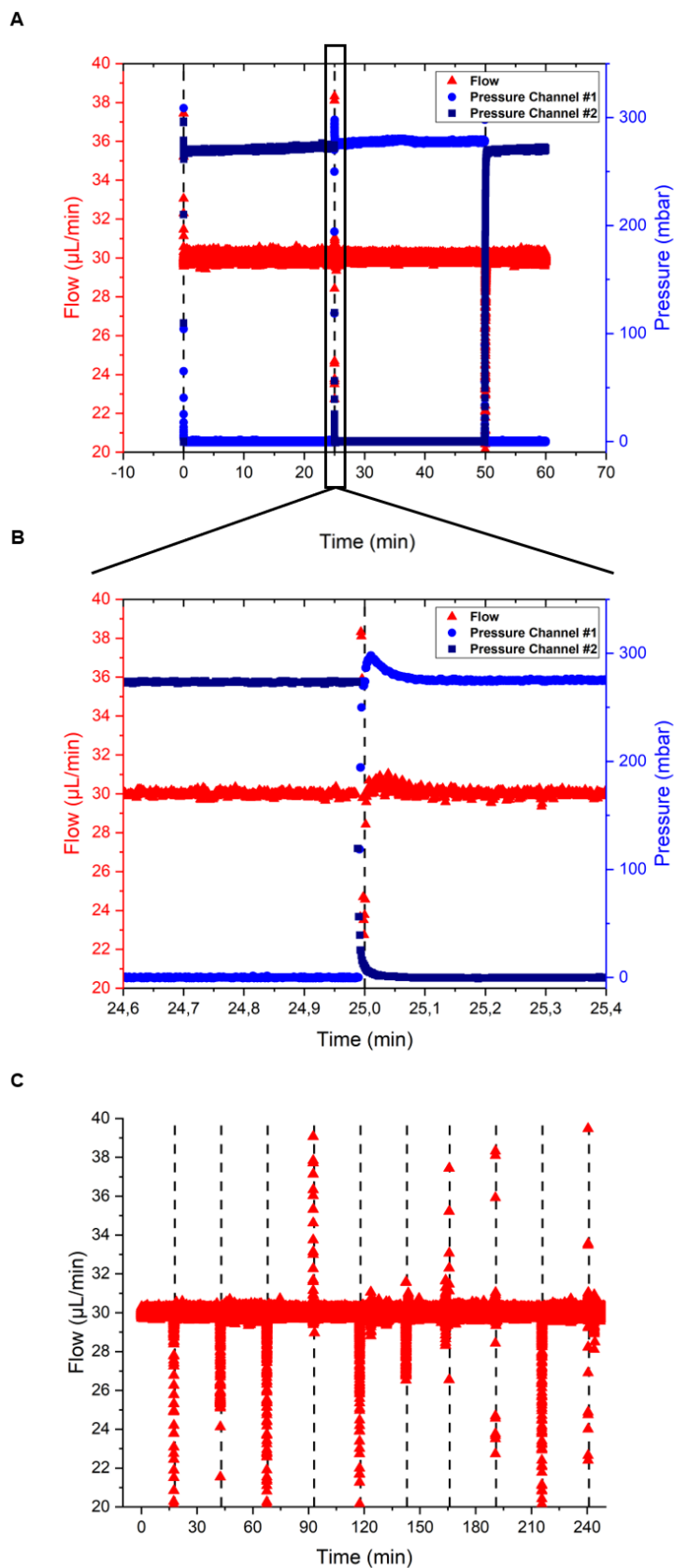


Figure 22: Representative flow output of the Fluigent circulation setup. Switch moments are indicated with dashed lines. A: A cycle of 50 minutes is shown, where after 25 minutes the L-switch changes position and a different pressure input channel is used. B: Exploded view of A. C: 4 h flow unit output results indicating long term flow stability.

Two factors that complicate the stability of the flow output are the responsiveness of the L-switch and the difficulty to obtain stable fluidic resistance. It has been observed at least once that the L-switch switches inadequately, leading up to a disturbed feedback loop. This mainly occurred in longer running (mostly 72 h) experiments. This resulted in a reversed flow direction, which in turn caused the flow unit to demand for a higher pressure, as the flow is set at a flow of +30 $\mu\text{L}/\text{min}$. Consequently, one of the reservoirs empties quickly, causing both disturbance of the volume balance in the reservoirs and, more importantly, huge amounts of shear stresses for the cells and sustained periods without nutrients as air is pumped through the channels. To limit the effects of this issue, a maximum pressure can be set. However, it is difficult to tweak this variable, as the fluidic resistance changes significantly upon introduction of microfluidic channels. After implementation of microfluidic channels in the circulation, the fluidic resistance increased, with values varying from $\sim 100\text{-}300$ mbar. Per channel, the microfluidic resistance is different. Additionally, small tubing is needed to connect the channels, leading up to increased fluidic resistance. If the maximum pressure value is set too high, errors in the circulation lead to almost instantaneous emptying of one of the reservoirs, killing the cells in the process. If the maximum pressure value is set too low, the flow rate cannot be kept stable at 30 $\mu\text{L}/\text{min}$. This differs per experiment, but mostly, a stable flow rate was obtained with a pressure < 500 mbar, so that the maximum pressure could be set at 500 mbar.

It is important to know whether the flow rate is high enough to provide the cells with sufficient nutrients. Since we can assume that the effective culture time (ECT) scales with the height of the medium (ECT $\sim h$), an estimation can be made based on the medium refreshment rate needed. [55] In a T75 flask, HUVECS are cultured up to 72 hours in a volume of 10 mL. This corresponds to a height of 1.33 mm. In a lumen of ~ 200 μm diameter (after VFP 400 μm x 400 μm channels), the height corresponds to the radius, but as a lumen is cylindrical, the value has to be corrected by 2π . To obtain roughly the same refreshment rate, the channel should be replenished with medium every ~ 52 min. The volume of one channel is roughly 0.31 μL . Thus, at a flow rate of 30 $\mu\text{L}/\text{min}$, the theoretical flow needed to obtain a ~ 5 dynes/cm² shear stress, is roughly 5000 times higher than needed to keep the cells viable. However, only one channel is considered in this case, without recirculation of medium. Within the first week of the experiment, this consideration is not expected to cause major problems regarding cell viability. Even with recirculation of medium and implementation of multiple designs, it is expected that the current volume used (~ 2.5 mL) is sufficient to keep the cells viable for at least a week.

The main problem that arises, however, is that cell medium can be stored best at 4°C to maintain growth factor stability. Medium is stable for up to a week at RT, so to keep the circulation stable for longer than 1 week, it is recommended to keep the medium at 4°C. [56] To this end, it may be beneficial to increase the tubing length, so that medium can be kept at 4°C outside the incubator and has sufficient time to be warmed up inside the incubator before reaching the cells.

4.2.2 Internal volume

As discussed in the platform requirements, an important parameter for the circulation is the internal volume. The tubing ID is 0.02 IN, meaning that the total internal volume per cm tubing is ~ 2 μL . In the complete setup, ~ 250 cm tubing is used. Furthermore, a ~ 15 cm piece of 127 ID tubing (PEEK) is used to increase the fluidic resistance, which contributes to a more stable flow output. The internal volume of the L-switch is 660 nL. [57] Per OoC, an additional ~ 0.31 μL of medium volume is present. The total internal volume inside the circulation (reservoirs not considered) is thus mainly accounted for by the tubing and is in total roughly 500 μL . This means that during each cycle, at least 500 μL of medium has to be displaced per reservoir. A displacement of 750 μL will be set per reservoir to prevent that the same medium is reused each cycle. In the circulation, 2 mL Eppendorf tubes are used as reservoirs. The left reservoir shown in Figure 14A will be filled with 1375 μL and the right reservoir with 625 μL . In further experiments, the circulation can be optimized in terms of internal volume by tweaking the ID, tubing length, and reservoir volume.

4.2.3 Sampling

Two distinct sampling protocols are needed: a protocol for routine sampling and a protocol for sampling at the end of the experiment. Routine sampling (for e.g. cytokines) can be performed by simply pausing the circulation and subtracting a small volume (e.g. 100 μL) out of the circulation and replacing the sampled volume with fresh medium. This protocol is presented in Supplementary Figure 3.

Apart from cytokines, CTCs are of great interest. The concentration of CTCs is generally low, so difficulties with detecting CTCs emerge when only a small volume will be sampled for analysis. [58] CTC sampling can be done by stopping the circulation, emptying the reservoirs, and flushing 500 μL of fresh medium (corresponding to the internal volume) through the circulation, whilst collecting the medium coming out of the circulation. This protocol is presented in Supplementary Figure 4.

4.3 Providing shear conditions

4.3.1 Syringe pump

Before implementation of the OoCs in the circulation, the shear was optimized using a syringe pump setup (shown in Figure 16). First, a variety of shear stresses was tested using lumens coated with HUVECs. Channel dimensions were $600\ \mu\text{m} \times 600\ \mu\text{m}$, with a lumen diameter corresponding to $\sim 400\ \mu\text{m}$, theoretically. Flow rates tested were 0.31, 0.83, 1.33, 2, 3, 4.24, 6.36, 14.4, and $30\ \mu\text{L}/\text{min}$. The results for the highest flow rates $14.4\ \mu\text{L}/\text{min}$ and $30\ \mu\text{L}/\text{min}$ (corresponding to a theoretical shear of ~ 0.3 and $\sim 0.6\ \text{dynes}/\text{cm}^2$, respectively) are shown in Supplementary Figure 6. It becomes evident that, while the viability and seeding density was good, the morphology of the cells was not shifted to spindle-like. In order to increase the shear stress, the channels were scaled down to $400\ \mu\text{m} \times 400\ \mu\text{m}$. Flow rates of $14.4\ \mu\text{L}/\text{min}$ and $30\ \mu\text{L}/\text{min}$ were assessed once again. It has to be noted that smaller channel dimensions result in decreased VFP efficacy and subsequent complications with cell seeding. However, as the flow unit (size M) used in the circulation can monitor flow rates up to $120\ \mu\text{L}/\text{min}$, a higher input flow rate is not possible. Therefore, it is chosen to scale down the channels to $400\ \mu\text{m} \times 400\ \mu\text{m}$.

Figure 23 shows the directionality and viability results obtained for a static control lumen and a lumen subjected to $30\ \mu\text{L}/\text{min}$ flow.

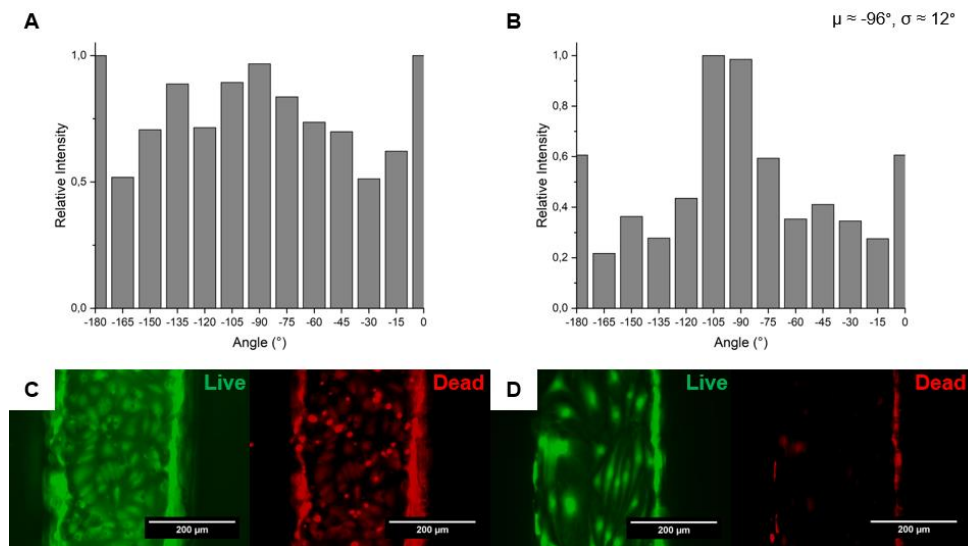


Figure 23: HUVEC directionality comparison for static and $30\ \mu\text{L}/\text{min}$ flow condition using a simple syringe pump setup (shown in Figure 16). A: directionality plot for static control sample (corresponding to live signal of C). B: directionality plot for flow sample (corresponding to live signal of D). C: static condition, Calcein-AM & Ethidium Homodimer-1 live/dead fluorescence output. D: Flow condition, Calcein-AM & Ethidium Homodimer-1 live/dead fluorescence output.

In Figure 23A+B it is presented that the lumen subjected to shear shows a population mean directionality of around -96° , whereas the control lumen shows no preferred directionality. The population mean and population standard deviation are depicted in Figure 23B (top right).

The slight deviation from -90° can be explained by the fact that the flow pattern might not be perfectly straight due to slight alterations in the smoothness of the lumen. Local narrowing of the lumen can namely lead to disturbed flow patterns, leading to changes in flow alignment direction. The increase in signal at $-180^\circ/0^\circ$ is an artifact due to the overlapping scale bar present in Figure 23C+D. The scale bar is removed in figures later processed. Figure 23C+D shows the live/dead viability images obtained from the corresponding lumens. The dead signal shows higher signal for the control than for the sample subjected to flow. This could be due to the continuous availability of fresh nutrients for the flow condition.

There seems to be a decrease in cell density upon introduction of flow. In literature, shear has been reported to slightly decrease cell density, whilst increasing endothelial barrier function. [34] It is however also very likely that the initial seeding density varied. In further experiments, the barrier function could be assessed. This is discussed later in section 6.

4.3.2 HUVECs in circulation

Then, flow was applied for 24 h using the circulation described before in section 4.1. Medium was supplied with 10 mM HEPES buffering. An overview of the results obtained is presented below in Figure 24. 4 control lumens are compared to 5 lumens subjected to shear stresses.

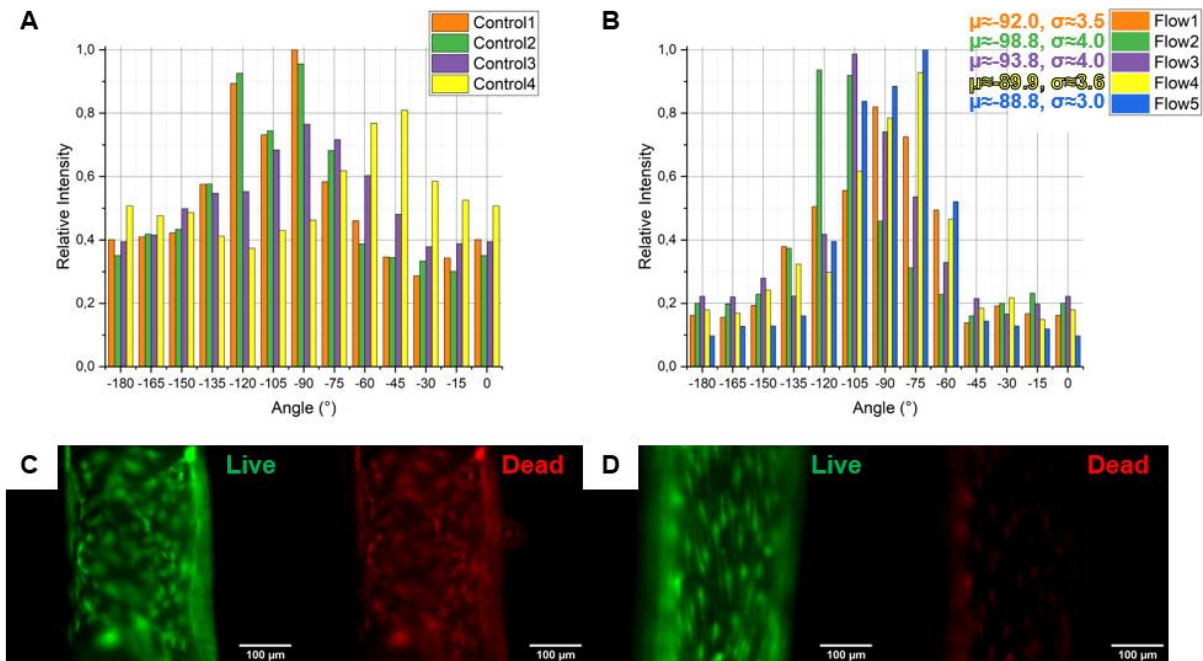


Figure 24: HUVEC directionality comparison for static and 30 µL/min flow conditions. A: Directionality plots for static control samples. B: Directionality plot for flow samples. C: Static condition, representative Calcein-AM & Ethidium Homodimer-1 live/dead fluorescence output. D: Flow condition, representative Calcein-AM & Ethidium Homodimer-1 live/dead fluorescence output.

Immediately, it becomes clear that there is an evident difference between flow and control conditions in terms of directionality (Figure 24A+B). This indicates that HUVECs align to the flow in the lumen. This is further illustrated in Figure 24C+D. Again, the population means and population standard deviations are depicted top right.

An additional overview of static and flow lumens is shown in Supplementary Figure 6. Figure 24C+D once again indicates that the dead signal is higher for the control lumen compared to the lumen subjected to shear. The mean intensity of the dead signal was quantified using ImageJ for all samples, but no significant overall change in intensity was observed. Again, it has to be noted that lumens were not confluent throughout the entire length of the channel. Seeding in small lumens remains to be the main cause for this problem as it was not observed for larger lumens of ~400 µm corresponding to 600 µm x 600 µm channels (representative overview shown in Supplementary Figure 5).

What becomes evident from Figure 24C+D is that the lumens are bigger than the expected diameter of ~200 μm . Lumen characterization in ImageJ was done by performing 3 measurements per lumen. 4 control and 5 lumens subjected to shear were assessed. A lumen size of $223.4 \pm 28.8 \mu\text{m}$ for the static lumens and $291.7 \pm 60.1 \mu\text{m}$ for the lumens to which flow was applied was observed. This is a significant difference compared to the theoretical value of 200 μm , as the flow applied (30 $\mu\text{L}/\text{min}$) should in theory correspond to a shear of ~1.6 dynes/cm^2 instead of 5 dynes/cm^2 . In theory, the flow applied to lumens of 290 μm should be ~90-95 $\mu\text{L}/\text{min}$ (Supplementary Figure 7). Inconsistency of the lumen diameter as well as possible leakiness of the vessel could both affect this value. The fact that HUVECs still behaved appropriately could be explained by the difference in experimental setup compared to literature. This cylindrical cell monolayer culture using a hydrogel (in this case collagen) is different compared to other HUVEC culturing methods reported. Furthermore, no supporting cells are introduced in the collagen. Supporting cells such as Mesenchymal Stem Cells and pericytes could greatly influence the rigidity and stability of the endothelial lineage. [59, 60] The significant difference ($P < 0.005$) in lumen size between control and flow could be explained by the variance in lumen seeding efficacy. The best looking lumens, with the highest initial seeding density, were picked for flow application. It could be the case that bigger lumens are easier to seed, and therefore result in better lumens.

Therefore, to improve upon the design in the future, it could be helpful to increase the channel cross-section. As discussed before, this would increase the desired flow input above the maximum threshold of 120 $\mu\text{L}/\text{min}$ for the flow unit (Supplementary Figure 6) but as a possible workaround the viscosity of the medium could be increased, e.g. using Xanthan Gum. Increased medium viscosity means relatively higher shear stresses at relatively lower flow rates. Van den Broek *et al.* showed that Xanthan Gum is a suitable additive for increasing medium viscosity. [61, 62] Dextran is more regularly used, but known to lower cell proliferation, as well as to increase the osmolality above the acceptable threshold for cells. [62] Another simpler option would be to scale up to a larger flow unit. A flow unit of size L can work with flow rates up to 1 mL/min . [63] It has to be noted that it is expected that the desired flow rate increases significantly, but, as flow has to be optimized for organ-specific endothelium in presence of the (tumor) microenvironment, it could be that lower flow rates are sufficient to provide adequate shear stresses.

Not only the lumen diameter deviates from the theoretical value, but also the channel characteristics differ. 10 channels were cut into slices and 3 size measurements were performed per cross-section in ImageJ. A representative image of a channel is shown in Supplementary Figure 8A. The width was measured to be $317.0 \pm 27.6 \mu\text{m}$ and the height $384.3 \pm 6.3 \mu\text{m}$. As the 3D printer used to produce the mold has a lateral resolution of 62.5 μm , the feature width should at least be 375 μm . The width is however significantly reduced. This strongly deviating value could be explained by the resolution of the 3D printer used.

Lumens presented a large variation in size overall. Incubation time between collagen introduction and medium introduction, inlet size, local collagen concentration (due to inadequate mixing), pH, as well as medium used to perform VFP (EGM-2 or PBS are both used) could all possibly influence the size of the lumen formed. [36]

All in all, despite variations in lumen diameter, lumens subjected to shear stresses presented great viability and spindle-like morphology. Static controls were still viable, but lack morphological changes, which is associated with worse recapitulation of *in vivo* endothelium.

4.3.3 HMECs in circulation

As discussed earlier, in the future a breast and bone marrow OoC will be designed. Instead of HUVECs, the organ specific breast endothelial cells, HMECs, were assessed using the circulation for 24 h at a flow rate of 30 $\mu\text{L}/\text{min}$. The results are shown in Figure 25.

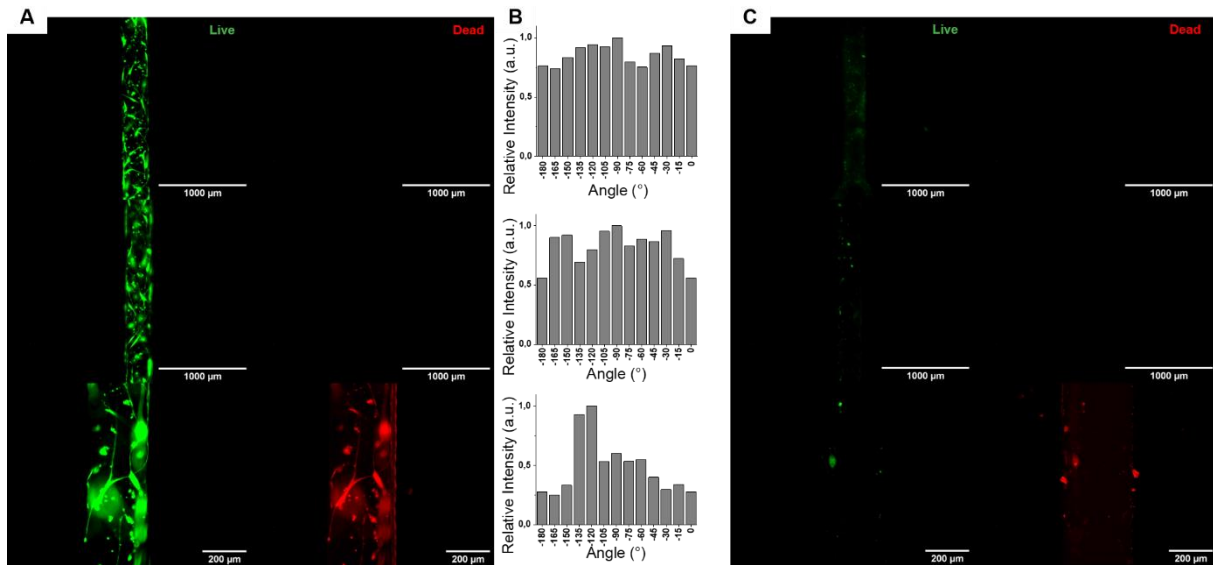


Figure 25: HMEC shear experiments using the circulation. A: static control B: Directionality plots corresponding to the live signal shown in A. C: lumens subjected to 30 $\mu\text{L}/\text{min}$ flow for 24 h.

It is presented in Figure 25A and Figure 25B that HMECs distributed randomly in absence of flow. The signal increase between -135° to -120° in the bottom plot of Figure 25B could be explained by the very bright cell dictating the distribution, shown in the left bottom of the accompanied live signal. Unfortunately, the cells seemed to have detached in the presence of flow. It could very well be the case that HMECs behaved completely different in the presence of shear. This would mean that the optimal shear stress for this cell type differs. It is important to note that the initial density of cells (shown in static control samples) was quite low. A fully established monolayer may be more stable. Furthermore, HMECs were cultured for only 24 h before flow application due to time restrictions. Increasing this time could enhance the integrity of the endothelial barrier. It is recommended to optimize the shear in presence of the tumor microenvironment, as this might lead to further alteration of the endothelial barrier. [28] Furthermore, as discussed before, the presence of pericytes could greatly alter the behavior of the endothelium. [60] Lumen diameter was measured by determining the lumen diameter from the top two live pictures in Figure 25A. 3 measurements were performed per lumen. The mean diameter was $291.2 \pm 12.5 \mu\text{m}$, a value similar to the mean obtained for the HUVECs in circulation experiment described before (Section 4.3.2). It is therefore hypothesized that the change in behavior is not caused by a change in lumen diameter, but rather by the variations in seeding density and cell type.

4.4 Breast tumor-on-a-chip characterization

In future research, aside from a vessel module, a tumor microenvironment has to be implemented. Communication between the vasculature and the microenvironment needs to be supported. As a proof of concept, the barrier integrity as well as the compatibility of cell seeding upon VFP is assessed. As a simplification, only one cell type is seeded in the chip. In the endothelial channel, 10 million cells/mL are seeded, whereas 5 million cells/mL are seeded in the hydrogel. Figure 26 presents the results obtained upon introduction of MDA-MB-231 cells in a single device.

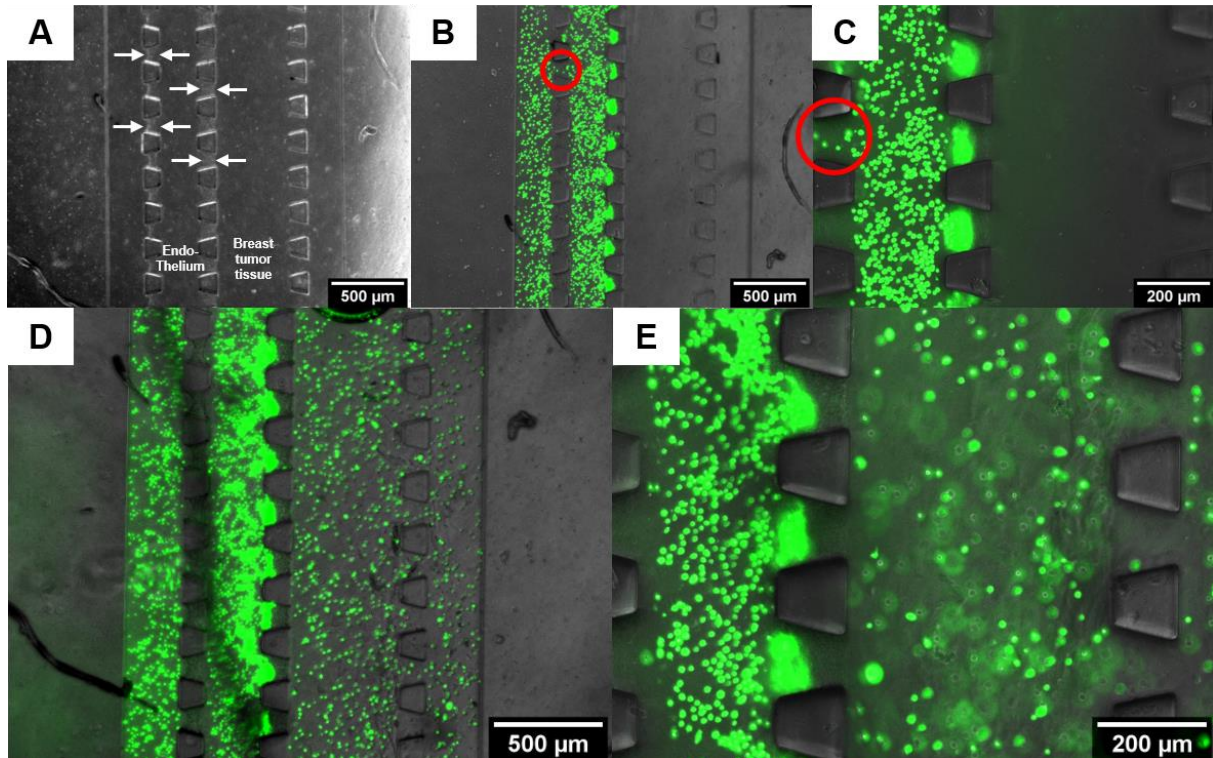


Figure 26: Overview of the breast Organ-on-a-chip upon introduction of MDA-MB-231 cells along with a green CellTracker. A: OoC after performing Viscous Finger Patterning. White arrows depict collagen between pillars. B-C: Overlay of transmitted and green fluorescent signal upon introduction of MDA-MB-231 cells. Due to a partial failure of the collagen, cells were able to travel to the side channel (as observed in the red circles). D-E: Overlay of transmitted and green fluorescent signal upon introduction of hydrogel containing MDA-MB-231 cells. Again, retention of the collagen between the vessel-hydrogel interface remains intact, whereas the hydrogel was permeated through the side channel. This time, cells migrated to the side channel at multiple sites.

First, 10 million cells/mL are introduced in medium in the endothelial channel (Figure 26B+C). It becomes clear that collagen prevents the cells to travel to the breast tumor microenvironment channel. Unfortunately, a rupture in the collagen caused the cells to travel to the side channels, designed for additional perfusion. Thereafter, cells were introduced in hydrogel at a final concentration of 5 million cells/mL (Figure 26D+E). A similar phenomenon is observed: the hydrogel between endothelium and hydrogel remained intact, but cells migrated to the side channels. In future designs, it might be beneficial to increase the resistance for the additional side perfusion channels by decreasing the space between pillars. Despite the difficulty to retain hydrogel barrier integrity, cells did not migrate from endothelium to breast tumor channel and vice versa. However, it seems as if there is no proper formation of a lumen. As seen in Figure 26, cells in the endothelium channel partially fill the gap between the pillars, meaning that introduction of endothelial cells would lead to a malformed endothelium channel. In effect, this worsens the homogeneity of the flow upon introduction of shear. Furthermore, it may be true that the hydrogel lumen is not cylindrical as VFP was possibly not performed successfully. The small size of the design makes VFP significantly more difficult to perform. It could possibly be the case that most of the hydrogel washed out of the channel thoroughly. In future designs, it might be helpful to decrease the thickness of the pillars, to improve homogeneity upon VFP.

The design presented is produced using SU8 lithography, which results in channel dimensions that are relatively small compared to the designs produced with the 3D printer. Using 10 channels and 3 measurements per channel, the width was determined to be $249.3 \pm 2.7 \mu\text{m}$ and the height $324.9 \pm 15.8 \mu\text{m}$. A representative cross-section is shown in Supplementary Figure 8B. Downscaling of the lumen is unfortunately not beneficial as VFP and subsequent cell seeding is then more complicated. Moreover, use of smaller channels leads to a significantly decreased flow (Supplementary Figure 7) and therefore poor mixing of medium in the circulation if the internal volume is still $\sim 500 \mu\text{L}$. It would be beneficial to use increased dimensions in further experiments, as this would be more compatible with VFP, subsequent cell seeding and flow application.

An optimized design is already produced in SolidWorks (Figure 27). This design is made in collaboration with Dr. A. Zuchowska. The design consists of 5 distinct channels. Outermost channels 1 and 5 are used for additional side perfusion of medium. the 2nd and 4th channel are vessel channels, whereas the middle channel (channel #3) is used for introduction of the microenvironment. In this case, next to MDA-MB-231 and HMF cells, HMECs could be co-cultured in channel #3 to enhance vascularization. In channel 2 and 4, pericytes could possibly be suspended in the collagen to better mimic *in vivo* vasculature. Due to the increased dimensions of this design the model is easier to handle, and features can be printed using the 3D printer. Interstitial flow can be established between the two vessels upon vascularization of the hydrogel. In further research, introduction of spheroids instead of a cell suspension could be performed to further elaborate on the relevance of the model.

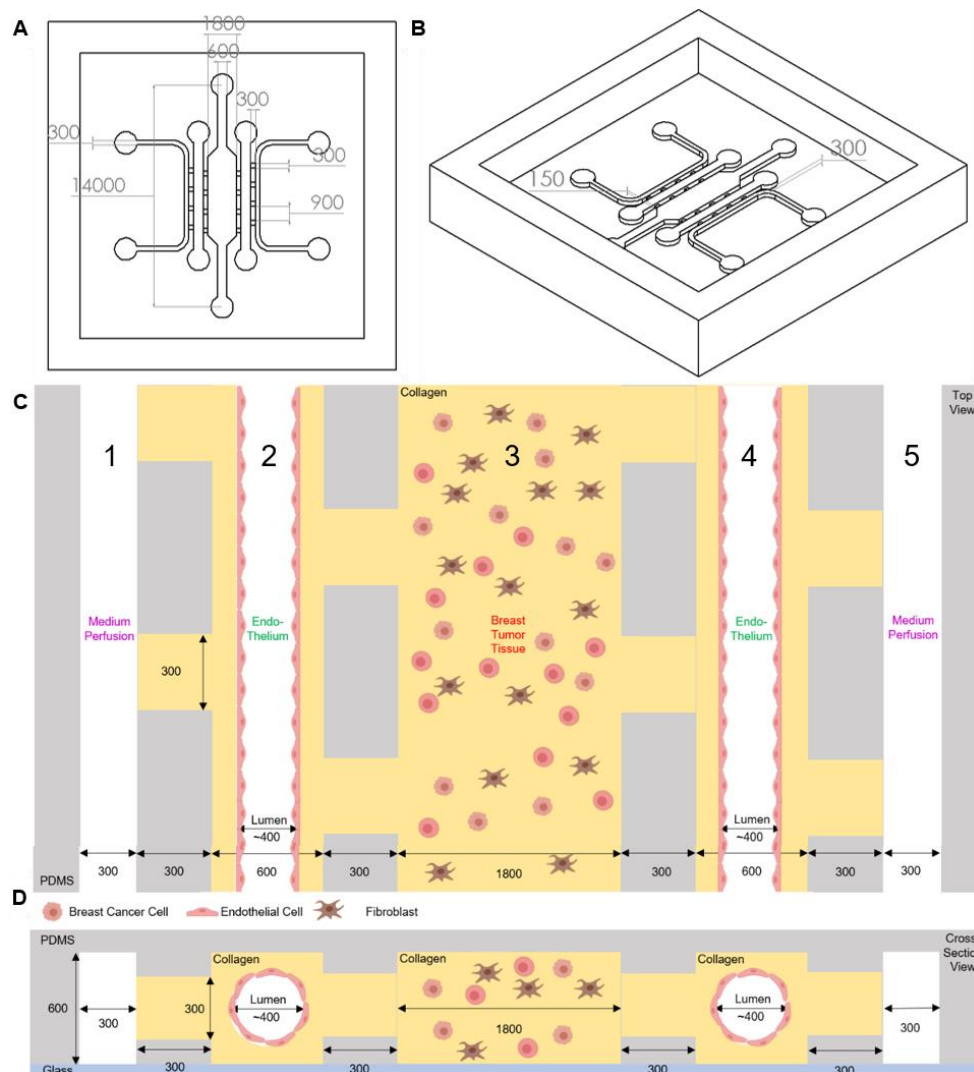


Figure 27: Overview of a novel breast tumor-on-a-chip design. A-B: SolidWorks overview of dimensions. C-D: Schematic overview of the design cultured with breast tumor microenvironment associated cell types. All dimensions in μm . Cells illustrated using BioRender.

5 Conclusions

An automated circulation that is suitable to establish cross-talk for a wide variety of OoC designs is presented. The circulation provides stable, unidirectional flow for at least 24 h as well as physiologically relevant shear stresses for at least 24 h. Sampling can be performed on-demand in an ongoing experiment for cellular and molecular analysis. Additionally, whole volume can be sampled at the end of an experiment.

Preliminary results show great viability and metabolic activity of HUVECs, HMECs, and HMF:MDA-MB-231 cells cultured at 3:1 or higher ratios of HMF using 10 mM HEPES for 96 h in 2D. However, HEPES should be used with caution, and further experiments should be performed to assess long-term buffering efficacy and biocompatibility in 3D environment.

A vessel OoC is designed and adequate shear stresses are provided using the circulation. It is shown that HUVECs in the OoC have spindle-like morphology and great viability after 24 h of flow application. The circulation is expected to be suitable for long-term experiments, as sufficient nutrients are available in the cell medium and flow output was stable. Preliminary results show that HMECs possibly behave differently in the presence of the same shear stresses applied to HUVECs, and therefore shear optimization has to be performed separately for this cell type. It is also hypothesized that endothelial response will be influenced by the microenvironment.

Additionally, a breast tumor-on-a-chip is proposed, aimed to mimic the breast tumor microenvironment. This design is compatible with a wide variety of cell types, and can thus also be used to produce other organ models such as a bone marrow module. It is recommended to increase feature dimensions for future research. An improved design is already designed and is yet to be tested.

The circulation designed is not only suitable for studying breast metastasis, but due to the versatility of the design, it can also pave the way towards establishment of a circulation that is compatible with virtually any OoC design. This way, organ cross-talk can be assessed for a wide variety of conditions.

6 Outlook

First of all, the circulation proves to be robust for 24 h with HUVECs, but long-term stability as well as long-term viability is not characterized as of yet. It is therefore recommended to assess long-term viability of the vessel-on-a-chip and breast tumor-on-a-chip models cultured in the circulation. Moreover, it is recommended to assess long-term stability of the flow output. Skardal et al. presented that upon 18 d of culturing in a circulation, gut cancer cells (HCT116 cells) migrated from the primary organ to secondary liver cells (HepG2 cells). [30] Intravasation and extravasation using vasculature was not considered in this study. It could therefore be very well the case that it would take >18 d for a MDA-MB-231 cell to successfully metastasize to bone tissue, and therefore a long-term stable circulation is essential. Further research should therefore aim to characterize on-chip metastasis rate as well.

Secondly, organ models are not fully established yet. Further improvements could aim at introduction of relevant cell types. In addition to cancer associated fibroblasts, for example, introduction of tumor associated macrophages could greatly improve the relevance of the model. Invasiveness has been shown to increase significantly upon introduction of macrophages. [64] In a review by Soysal et al., the relevance of the role of immune cells in the breast tumor microenvironment is emphasized. The interplay is shown in Figure 28. Additionally, as discussed before, pericytes could be introduced to increase the stability of the endothelium.

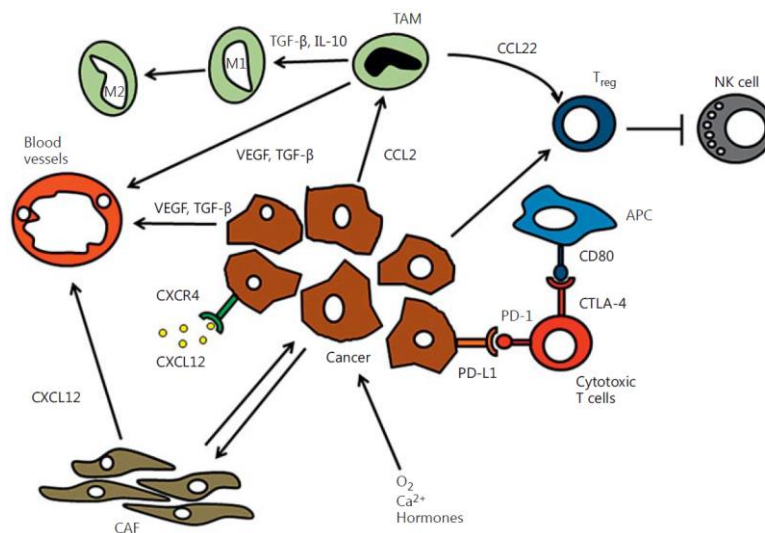


Figure 28: Overview of the breast tumor microenvironment emphasizing the role of the immune system and other cell types. From [65].

Flow has to be optimized for a circulation in which HMECs as well as bone marrow endothelium is present. As discussed before, it could be very well the case that the optimal shear for these cell types is different than the optimal flow rate for HUVECs. Therefore, to optimize the flow, step-wise increasing flow can be applied. Live imaging is recommended to study cellular responses to the flow. This way, the maximum flow rate to be applied could be determined more easily.

As mentioned before, it has been observed that the L-switch does not always function. It is therefore recommended to replace the L-switch for a newer version to avoid possible issues.

Currently, HEPES is used to obtain CO₂-independent culture medium. In future research, however, it would be beneficial to use conventional culture medium and 5% CO₂. HEPES has proven to be sufficiently biocompatible to maintain cell viability and growth for 96 h in 2D culture, but long-term effects remain unclear. Moreover, culturing of high ratios of MDA-MB-231 cells with respect to Human Mammary Fibroblasts is not recommended due to their high metabolic activity. Additionally, the buffering capacity and biocompatibility of HEPES has not been tested in a 3D environment and therefore remains to be determined. It is recommended to perform further experiments using either a conventional incubator, or by supplying the Ibidi stage-top incubator with CO₂.

When a working OoC is established, further research should aim to characterize the circulation based on feasibility to measure cytokines and CTCs. Firstly, it is relevant to know what the concentration of key cytokines involved in breast cancer progression is in the circulation, so that the internal volume of the circulation can be optimized further. The ability to measure cytokine concentrations over time would greatly increase the relevance of the circulation. The concentration of cytokines should not be too low, as factors need to be able to build up in the system and reach biologically relevant thresholds to function similar to an *in vivo* tumor microenvironment. A good cytokine to start with would be interleukin 6 (IL-6). IL-6 is a cytokine known to induce proliferation and a more aggressive phenotype in estrogen receptor (ER) positive cells such as the MDA-MB-231 cell line used. [66] By culturing a breast OoC in the circulation, and subtracting 100 μL of medium daily whilst introducing fresh medium, the increase in IL-6 concentration can be determined over time. The sensitivity of an Enzyme-Linked Immunosorbent Assay (ELISA) for IL-6 is 0.7 pg/mL, whereas the assay range is 3.1-300 pg/mL. [35] The volume needed for such an assay is 100 μL , so either 100 μL will be sampled directly from the circulation, or a smaller sample volume will be diluted. As other markers, such as TGF- β , IL-1(β), IL-8, and IL-20, among others, are also known to play a role in breast tumor progression, it could be beneficial to perform a multiplexed ELISA to screen for multiple tumor markers. [67, 68]

The circulation needs to be optimized in terms of internal volume based on the outcome of performed ELISAs. Internal volume can be tweaked by lowering the volume inside the reservoirs, or by decreasing tubing length and inner diameter. Decreasing of the inner diameter has to be done with caution, as it can lead to a too high microfluidic resistance. The microfluidic resistance R scales with diameter d as follows:

$$R \sim \frac{1}{d^4}$$

This means that decreasing tubing inner diameter to 250 μm (which is roughly half the diameter of the tubing of ID 0.02 IN used) increases the resistance by a factor of ~ 16 . Additionally, cells can clog easier in decreased tubing dimensions. The internal volume V of the tubing scales with the radius of the tubing r as follows:

$$V \sim r^2$$

Therefore, internal volume is decreased roughly fourfold with such a decrease in tubing inner diameter. In case the resistance becomes too high, 2000 mbar is not sufficient to reach the demanded flow rate. Then, there is either a need to further decrease tubing length or to use a more powerful pump.

If troubles regarding the internal volume of the circulation would remain, there might be other solutions to avoid excessive factor dilution. A microfluidic platform presented by Cook et al. implements simple building blocks in an impeller pump actuated microfluidic circuitry. [69] The impeller pump is magnetically driven by a computer and allows physiologically relevant flow. This system allows for fast, reproducible, and accessible fabrication. It is easy to use and versatile.

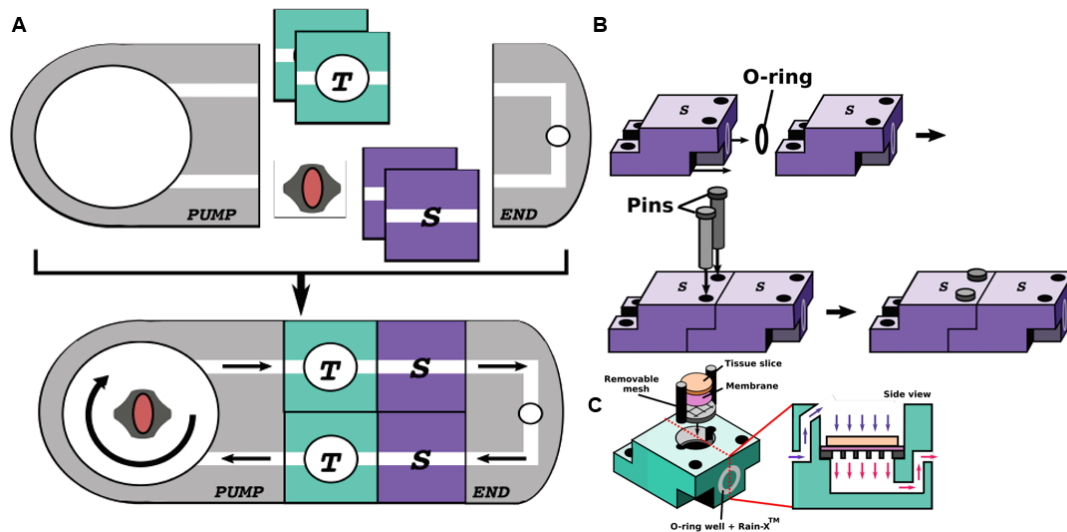


Figure 29: 3D printed Integrated Microfluidic platform. A: Schematic overview of the platform. A microfluidic impeller pump is integrated in the system, allowing controllable fluid flow in physiological ranges. Tissue blocks (green T) can be combined with simple straight channel blocks (blue S). B: Overview of connection of building blocks. C: Overview of a tissue building block. Adapted from [69].

Furthermore, CTCs are of great interest. Key mechanisms that should be recapitulated by the circulation are intravasation and extravasation. First of all, intravasation rate could be examined by introducing stained breast cancer cells in the breast OoC hydrogel. Then, the intravasation can be monitored over time by imaging the amount of cancer cells migrating towards the blood vessel over time. Extravasation can be quantified by manually introducing stained cancer cells through the blood vessel of a bone OoC. Again, live imaging can be performed to examine homing of cancer cells in the bone environment.

In later experiments, total CTC counts in the circulation can be performed by sampling and subsequent FACS analysis. A specialized single cell trapping column such as the VyCap trapping system could also be used. [70] The VyCap system consists of a microsieve. Upon capturing of a single cell in a pore of the microsieve, flow through this pore is blocked. This way, only 1 cell can settle per pore. Single cells can be counted and analyzed afterwards. This technique is very suitable for CTC sampling if the circulation is fully established.

An important parameter that has to be quantified in the future is the barrier integrity of the endothelium. A functioning barrier is namely very relevant, as CTCs can extravasate more easily in absence of a proper endothelial barrier. To this end, VE-cadherin stain can be added to the lumens to characterize the presence of tight-junctions. Furthermore, a fluorescent dye such as Dextran-FITC can be introduced in the lumen, so that the retention of the dye inside the lumen can be examined. These experiments have not been performed in this report, as the lumens did not show sufficient seeding densities to provide a stable monolayer as of yet.

7 Acknowledgements

I want to thank Dr. A. Zuchowska for her continuous support and daily supervision during my project. Her assistance was always there when needed most, both inside and outside the lab. The continuous supervision during my project by Prof. Dr. S. Le Gac was very much appreciated. I want to thank her in particular for loads of excellent, thorough, and helpful feedback. Furthermore, I want to thank C.A. Paggi for sharing his practical expertise in the lab and for countless discussions. Also thanks to him for co-designing, drawing and producing the design presented in section 3.1.2. Components of the circulation were kindly provided by Fluigent. Special thanks to William César from Fluigent for his continuous involvement and support throughout the project. I would like to thank Prof. Dr. L.W.W.M. Terstappen for taking part in my graduation committee and for his feedback on my progress during my thesis. Lastly, I want to thank the members and students of the AMBER and DBE group.

8 References

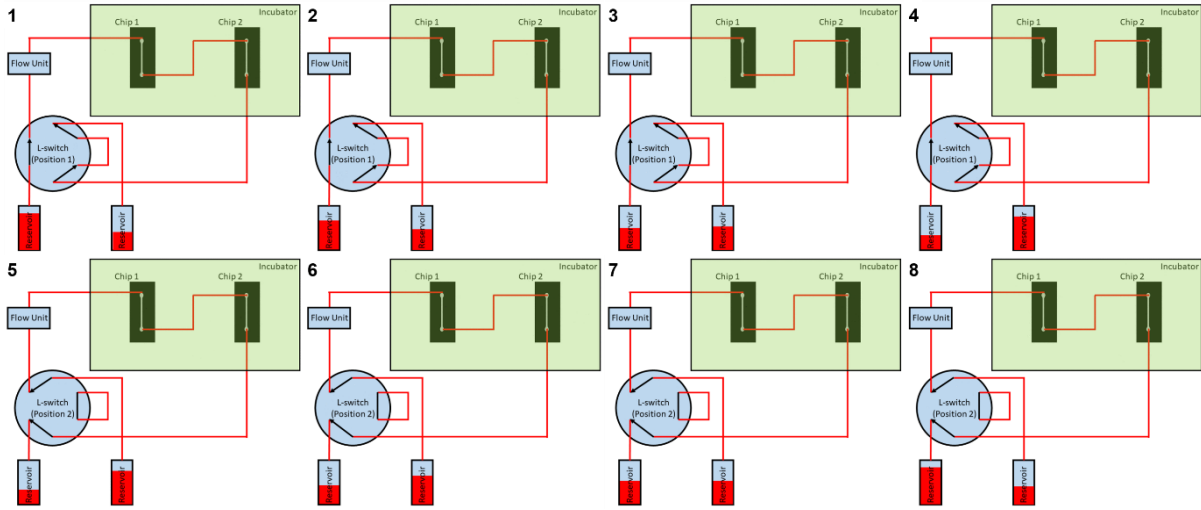
- [1] "Global Cancer Incidence: Both Sexes," 2018. <https://www.wcrf.org/dietandcancer/cancer-trends/worldwide-cancer-data> (accessed Nov. 11, 2020).
- [2] A. G. Waks and E. P. Winer, "Breast Cancer Treatment," *JAMA*, vol. 321, no. 3, p. 288, Jan. 2019, doi: 10.1001/jama.2018.19323.
- [3] "Breast Cancer," *World Health Organisation*. <https://www.who.int/cancer/prevention/diagnosis-screening/breast-cancer/en/> (accessed Mar. 16, 2020).
- [4] L. Chaffer, C and A. Weinberg, R, "A Perspective on Cancer Cell Metastasis," pp. 1559–1565, 2011.
- [5] X. Guan, "Cancer metastases: challenges and opportunities," *Acta Pharm. Sin. B*, vol. 5, no. 5, pp. 402–418, Sep. 2015, doi: 10.1016/j.apsb.2015.07.005.
- [6] K. A. Rejniak, T. H. Lee, and M. Cancer, "Circulating Tumor Cells: When a Solid Tumor Meets a Fluid Microenvironment," *Adv Exp Med Biol*, vol. 936, pp. 93–106, 2016, doi: 10.1007/978-3-319-42023-3.
- [7] A. F. Chambers, A. C. Groom, and I. C. MacDonald, "Dissemination and growth of cancer cells in metastatic sites," *Nat. Rev. Cancer*, vol. 2, no. 8, pp. 563–572, 2002, doi: 10.1038/nrc865.
- [8] X. Guan, "Cancer metastases: challenges and opportunities," *Acta Pharm. Sin. B*, vol. 5, no. 5, pp. 402–418, Sep. 2015, doi: 10.1016/j.apsb.2015.07.005.
- [9] F. Font-Clos, S. Zapperi, and C. A. M. La Porta, "Blood Flow Contributions to Cancer Metastasis," *iScience*, vol. 23, no. 5, May 2020, doi: 10.1016/j.isci.2020.101073.
- [10] D. Ribatti, G. Mangialardi, and A. Vacca, "Stephen Paget and the 'seed and soil' theory of metastatic dissemination," *Clin. Exp. Med.*, vol. 6, no. 4, pp. 145–149, Dec. 2006, doi: 10.1007/s10238-006-0117-4.
- [11] S. Paget, "The distribution of secondary growths in cancer of the breast," *Cancer metastasis*, vol. 8, no. 2, pp. 98–101, 1889.
- [12] D. L. Priwitaningrum *et al.*, "Tumor stroma-containing 3D spheroid arrays: A tool to study nanoparticle penetration," *J. Control. Release*, vol. 244, pp. 257–268, 2016, doi: 10.1016/j.jconrel.2016.09.004.
- [13] R. C. Dandekar, A. V Kingaonkar, and G. S. Dhabekar, "Role of macrophages in malignancy," *Ann Maxillofac Surg*, vol. 1, no. 2, pp. 150–154, 2011.
- [14] Q. Liu, H. Zhang, X. Jiang, C. Qian, Z. Liu, and D. Luo, "Factors involved in cancer metastasis : a better understanding to ' seed and soil ' hypothesis," *Mol. Cancer*, pp. 1–19, 2017, doi: 10.1186/s12943-017-0742-4.
- [15] A. C. Obenauf and J. Massagué, "Surviving at a Distance: Organ-Specific Metastasis," *Trends in Cancer*, vol. 1, no. 1, pp. 76–91, Sep. 2015, doi: 10.1016/j.trecan.2015.07.009.
- [16] G. L. Nicolson, "Organ specificity of tumor metastasis : role of preferential adhesion , invasion and growth of malignant cells at specific secondary sites," *cancer and metastasis*, vol. 188, pp. 143–188, 1988.
- [17] L. R. Patel, D. F. Camacho, Y. Shiozawa, K. J. Pienta, and R. S. Taichman, "Mechanisms of cancer cell metastasis to the bone: a multistep process," *Futur. Oncol.*, pp. 1285–1297, 2011.
- [18] G. Trujillo-de Santiago *et al.*, "The Tumor-on-Chip: Recent Advances in the Development of Microfluidic Systems to Recapitulate the Physiology of Solid Tumors," *Materials (Basel)*, vol. 12, no. 18, p. 2945, Sep. 2019, doi: 10.3390/ma12182945.
- [19] R. Sharma, "Breast cancer incidence, mortality and mortality-to-incidence ratio (MIR) are associated with human development, 1990–2016: evidence from Global Burden of Disease Study 2016," *Breast Cancer*, vol. 26, no. 4, pp. 428–445, 2019, doi: 10.1007/s12282-018-00941-4.
- [20] Y. Zhao, R. Kankala, S.-B. Wang, and A.-Z. Chen, "Multi-Organs-on-Chips: Towards Long-Term Biomedical Investigations," *Molecules*, vol. 24, no. 4, p. 675, Feb. 2019, doi: 10.3390/molecules24040675.
- [21] D. Huh *et al.*, "Acoustically detectable cellular-level lung injury induced by fluid mechanical stresses in microfluidic airway systems," *PNAS*, vol. 104, no. 48, pp. 18886–18891, 2007.

- [22] G. Kaushik, J. Leijten, and A. Khademhosseini, "Concise Review: Organ Engineering: Design, Technology, and Integration," *Stem Cells*, vol. 35, no. 1, pp. 51–60, Jan. 2017, doi: 10.1002/stem.2502.
- [23] B. Zhang, A. Korolj, B. F. L. Lai, and M. Radisic, "Advances in organ-on-a-chip engineering," *Nat. Rev. Mater.*, vol. 3, no. 8, pp. 257–278, Aug. 2018, doi: 10.1038/s41578-018-0034-7.
- [24] Y. Nashimoto *et al.*, "Vascularized cancer on a chip : The effect of perfusion on growth and drug delivery of tumor spheroid," *Biomaterials*, 2019, doi: 10.1016/j.biomaterials.2019.119547.
- [25] S. Nagaraju, D. Truong, G. Mouneimne, and M. Nikkhah, "Microfluidic Tumor – Vascular Model to Study Breast Cancer Cell Invasion and Intravasation," *Adv. Healthc. Mater.*, vol. 1701257, pp. 1–12, 2018, doi: 10.1002/adhm.201701257.
- [26] S. Bersini *et al.*, "A Microfluidic 3D In Vitro Model for Specificity of Breast Cancer Metastasis to Bone," *Biomaterials*, vol. 35, no. 8, pp. 2454–2461, 2015, doi: 10.1016/j.biomaterials.2013.11.050.A.
- [27] A. Marturano-kruik, M. Maria, K. Yeager, A. Chramiec, L. Hao, and S. Robinson, "Human bone perivascular niche-on-a-chip for studying metastatic colonization," 2017, doi: 10.1073/pnas.1714282115.
- [28] J. S. Jeon *et al.*, "Human 3D vascularized organotypic microfluidic assays to study breast cancer cell extravasation," *Med. Sci. Eng.*, vol. 112, no. 7, pp. 214–219, 2015, doi: 10.1073/pnas.1501426112.
- [29] J. Aleman and A. Skardal, "A multi - site metastasis - on - a - chip microphysiological system for assessing metastatic preference of cancer cells," *Biotechnol. Bioeng.*, no. October 2018, pp. 936–944, 2019, doi: 10.1002/bit.26871.
- [30] A. Skardal, M. Devarasetty, S. Forsythe, A. Atala, and S. Soker, "A reductionist metastasis-on-a-chip platform for in vitro tumor progression modeling and drug screening," *Biotechnol. Bioeng.*, vol. 113, no. 9, pp. 2020–2032, 2016, doi: 10.1002/bit.25950.
- [31] A. Skardal *et al.*, "Multi-tissue interactions in an integrated three-tissue organ-on-a- chip platform," *Nat. Sci. reports*, no. April, pp. 1–16, 2017, doi: 10.1038/s41598-017-08879-x.
- [32] D. A. Chistiakov, A. N. Orekhov, and Y. V. Bobryshev, "Effects of shear stress on endothelial cells: go with the flow," *Acta Physiol.*, vol. 219, no. 2, pp. 382–408, Feb. 2017, doi: 10.1111/apha.12725.
- [33] J. G. Destefano, A. Williams, A. Wnorowski, N. Yimam, C. Peter, and A. D. Wong, "Real-time quantification of endothelial response to shear stress and vascular modulators," *Integr. Biol.*, vol. 9, no. 4, pp. 362–374, 2018, doi: 10.1039/c7ib00023e.Real-time.
- [34] Y. I. Wang and M. L. Shuler, "UniChip enables long-term recirculating unidirectional perfusion with gravity-driven flow for microphysiological systems," *Lab Chip.*, vol. 18, no. 17, pp. 2563–2574, 2019, doi: 10.1039/c8lc00394g.UniChip.
- [35] "Human IL-6 Quantikine ELISA Kit." https://www.rndsystems.com/products/human-il-6-quantikine-elisa-kit_d6050#product-details (accessed Sep. 25, 2020).
- [36] L. L. Bischel, S. Lee, and D. J. Beebe, "A Practical Method for Patterning Lumens through ECM Hydrogels via Viscous Finger Patterning," *Lab. Autom.*, vol. 17, no. 2, pp. 96–103, 2012, doi: 10.1177/2211068211426694.A.
- [37] S. K. Y. Tang and G. M. Whitesides, "Basic Microfluidic and Soft Lithographic Techniques," in *Optofluidics: fundamentals, devices, and applications*, 2009, pp. 7–32.
- [38] M. A. Eddings, M. A. Johnson, and B. K. Gale, "Determining the optimal PDMS – PDMS bonding technique for microfluidic devices," *Micromech. Microeng.*, vol. 067001, 2008, doi: 10.1088/0960-1317/18/6/067001.
- [39] E. C. Cruz, "Cell line profile MDA-MB-231 (ECACC catalogue no. 92020424)," *Eur. Collect. Authenticated Cell Cult.*, 2017, [Online]. Available: https://www.phe-culturecollections.org.uk/products/celllines/generalcell/detail.jsp?refId=85120602&collection=ecacc_gc
- [40] J. Cooper, "CO2 concentration and pH control in the cell culture laboratory," *Public Health England*, 2019. <https://www.phe-culturecollections.org.uk/> (accessed Jan. 07, 2021).

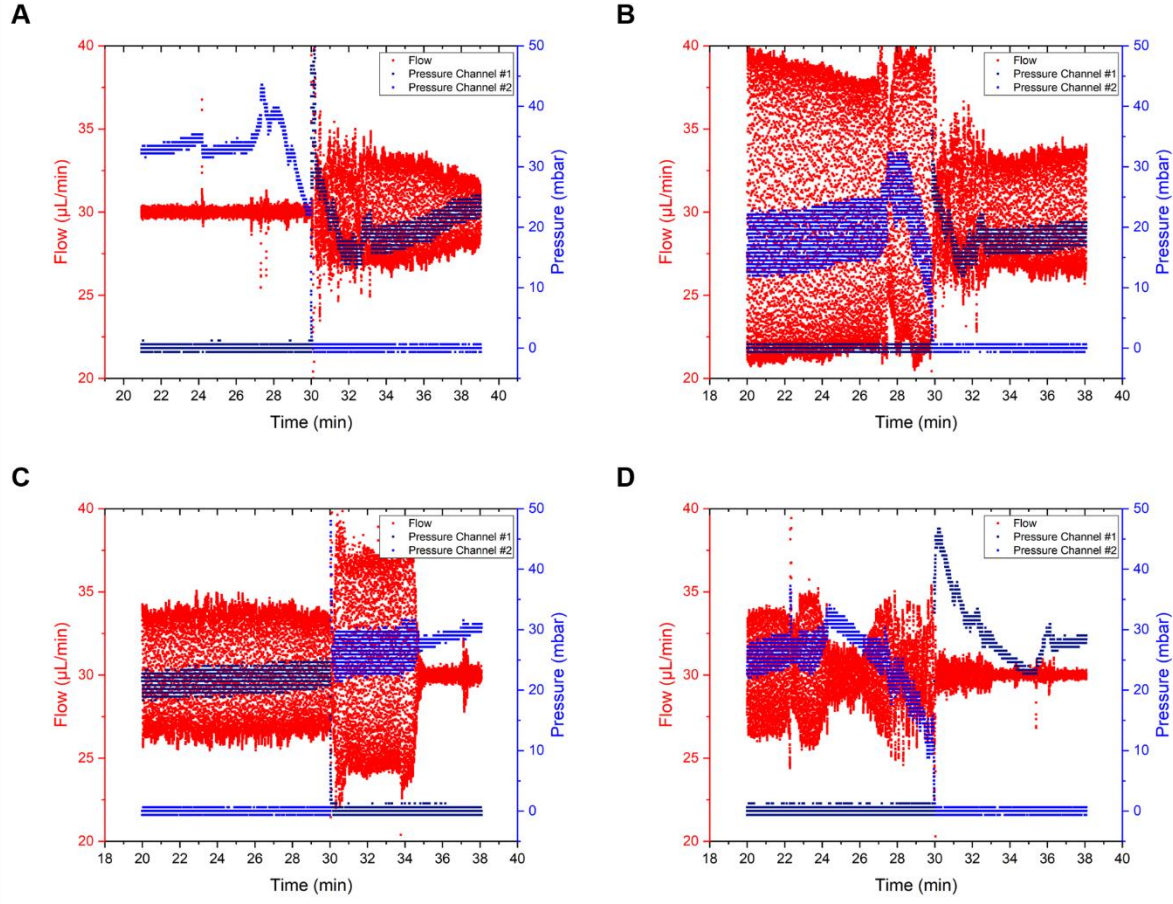
- [41] "HEPES Buffer Solution (1M)," *R&D systems*. https://www.rndsystems.com/products/hepes-buffer-solution-1-m-_b35110 (accessed Jan. 07, 2021).
- [42] R. Steward, D. Tambe, C. C. Hardin, R. Krishnan, and J. J. Fredberg, "Fluid shear, intercellular stress, and endothelial cell alignment," *Physiol Cell Physiol*, 2015, doi: 10.1152/ajpcell.00363.2014.
- [43] Y. Yang, P. Fathi, G. Holland, D. Pan, N. S. Wang, and M. B. Esch, "Pumpless Microfluidic Devices for Generating Healthy and Diseased Endothelia," *Lab Chip*, 2019, doi: 10.1039/C9LC00446G.
- [44] A. D. Van Der Meer, A. A. Poot, J. Feijen, and I. Vermes, "Analyzing shear stress-induced alignment of actin filaments in endothelial cells with a microfluidic assay," *Biomicrofluidics*, pp. 1–5, 2010, doi: 10.1063/1.3366720.
- [45] I. Pereiro, A. Fomitcheva Khartchenko, L. Petrini, and G. V. Kaigala, "Nip the bubble in the bud: A guide to avoid gas nucleation in microfluidics," *Lab Chip*, vol. 19, no. 14, pp. 2296–2314, 2019, doi: 10.1039/c9lc00211a.
- [46] C. M. Bowman, E. M. Berger, E. N. Butler, K. M. Toth, and J. E. Repine, "HEPES May Stimulate Cultured Endothelial Cells To Make Growth-Retarding Oxygen Metabolites," *Vitr. Cell. Dev. Biol.*, vol. 21, no. 3, pp. 9–11, 1985.
- [47] C. N. Gutt, Z. G. Kim, D. Hollander, T. Bruttel, and M. Lorenz, "CO2 environment influences the growth of cultured human cancer cells dependent on insufflation pressure," *Surg. Endosc.*, vol. 15, pp. 314–318, 2001, doi: 10.1007/s004640000321.
- [48] J. S. Zigler Jr., J. L. Lepe-Zuniga, B. Vistica, and I. Gery, "Analysis of the cytotoxic effects of light-exposed hepes-containing culture medium," *Vitr. Cell. Dev. Biol. Vol.*, vol. 21, no. 5, pp. 1–6, 1985, doi: <https://doi.org/10.1007/BF02620943>.
- [49] C. R. Kruse, M. Singh, S. Targosinski, J. A. Sørensen, E. Eriksson, and K. Nuutila, "The effect of pH on cell viability , cell migration , cell proliferation , wound closure and wound re-epithelialization : in vitro and in vivo study," *Wound Repair Regen.*, vol. 25, no. 2, pp. 260–269, 2017, doi: 10.1111/wrr.12526.
- [50] D. D. Truong *et al.*, "A human organotypic microfluidic tumor model permits investigation of the interplay between patient-derived fibroblasts and breast cancer cells," *Cancer Res.*, vol. 79, no. 12, pp. 3139–3151, 2019, doi: 10.1158/0008-5472.CAN-18-2293.
- [51] N. Eiro *et al.*, "Cancer-associated fibroblasts affect breast cancer cell gene expression, invasion and angiogenesis," *Cell. Oncol.*, vol. 41, no. 4, pp. 369–378, 2018, doi: 10.1007/s13402-018-0371-y.
- [52] S. Y. Jeong, J. H. Lee, Y. Shin, S. Chung, and H. J. Kuh, "Co-culture of tumor spheroids and fibroblasts in a collagen matrix-incorporated microfluidic chip mimics reciprocal activation in solid tumor microenvironment," *PLoS One*, vol. 11, no. 7, pp. 1–17, 2016, doi: 10.1371/journal.pone.0159013.
- [53] M. Nguyen *et al.*, "Dissecting Effects of Anti-cancer Drugs and Cancer-Associated Fibroblasts by On-Chip Reconstitution of Immunocompetent Tumor Microenvironments," *Cell Rep.*, vol. 25, no. 13, pp. 3884–3893.e3, 2018, doi: 10.1016/j.celrep.2018.12.015.
- [54] H. Jaganathan *et al.*, "Three-Dimensional In Vitro Co-Culture Model of Breast Tumor using Magnetic Levitation," *Sci. Rep.*, vol. 6468, pp. 1–9, 2014, doi: 10.1038/srep06468.
- [55] H. Craighead and P. Yang, "From microfluidic application to nanofluidic phenomena issue," *Chem. Soc. Rev.*, vol. 39, no. 3, pp. 1036–1048, 2010, doi: 10.1039/b909900j.
- [56] PromoCell, "Endothelial Cell Growth Medium 2: Technical Library." https://www.promocell.com/product/endothelial-cell-growth-medium-2/#tab-technical_library (accessed Nov. 25, 2020).
- [57] Fluigent Smart Microfluidics, "L-Switch™." <https://www.fluigent.com/product/microfluidic-components-3/l-switch/> (accessed Mar. 02, 2020).
- [58] W. He *et al.*, "Quantitation of circulating tumor cells in blood samples from ovarian and prostate cancer patients using tumor-specific fluorescent ligands," *Int. J. Cancer*, vol. 123, no. 8, pp. 1968–1973, 2009, doi: 10.1002/ijc.23717. Quantitation.

- [59] T. O. Pedersen *et al.*, “Mesenchymal stem cells induce endothelial cell quiescence and promote capillary formation,” *Stem Cell Res. Ther.*, pp. 1–10, 2014.
- [60] G. Bergers and S. Song, “The role of pericytes in blood-vessel formation and maintenance,” *Neuro. Oncol.*, vol. 7, pp. 452–464, 2005, doi: 10.1215/S1152851705000232.
- [61] C. N. van den Broek, R. A. A. Pullens, O. Frøbert, M. C. M. Rutten, W. F. den Hartog, and F. N. van de Vosse, “Medium with blood-analog mechanical properties for cardiovascular tissue culturing,” *Biorheology*, vol. 45, no. 6, pp. 651–661, 2008, doi: 10.3233/BIR-2008-0513.
- [62] C. N. Van Den Broek, M. C. M. Rutten, and F. N. Van De Vosse, “Creation of a culture medium with blood analog mechanical properties,” *Cardiovasc. Biomech.*, vol. 264, p. 5612, 2005.
- [63] “FRP: Flow-Rate Platform.” <https://www.fluigent.com/product/microfluidic-components/frp-flow-rate-platform/> (accessed Nov. 27, 2020).
- [64] S. Mi, Z. Liu, Z. Du, X. Yi, and W. Sun, “Three-dimensional microfluidic tumor–macrophage system for breast cancer cell invasion,” *Biotechnol. Bioeng.*, vol. 116, no. 7, pp. 1731–1741, 2019, doi: 10.1002/bit.26961.
- [65] S. D. Soysal, A. Tzankov, and S. E. Muenst, “Role of the Tumor Microenvironment in Breast Cancer,” *Pathobiology*, vol. 82, no. 3–4, pp. 142–152, 2015, doi: 10.1159/000430499.
- [66] X. Dai, H. Cheng, Z. Bai, and J. Li, “Breast Cancer Cell Line Classification and Its Relevance with Breast Tumor Subtyping,” *Cancer*, vol. 8, 2017, doi: 10.7150/jca.18457.
- [67] L. A. Méndez-García *et al.*, “Breast Cancer Metastasis: Are Cytokines Important Players During Its Development and Progression?,” *J. Interf. Cytokine Res.*, vol. 39, no. 1, pp. 39–55, Jan. 2019, doi: 10.1089/jir.2018.0024.
- [68] M. Esquivel-Velázquez, P. Ostoa-Saloma, M. I. Palacios-Arreola, K. E. Nava-Castro, J. I. Castro, and J. Morales-Montor, “The Role of Cytokines in Breast Cancer Development and Progression,” *J. Interf. Cytokine Res.*, vol. 35, no. 1, pp. 1–16, Jan. 2015, doi: 10.1089/jir.2014.0026.
- [69] S. R. Cook and R. R. Pompano, “A 3D-Printed Modular Microchip With an Integrated Impeller Pump to Model Inter-Organ Communication,” 2020.
- [70] “Filtration disposable,” *VyCAP*. <https://www.vycap.com/product/filter-ctc/> (accessed Mar. 28, 2020).

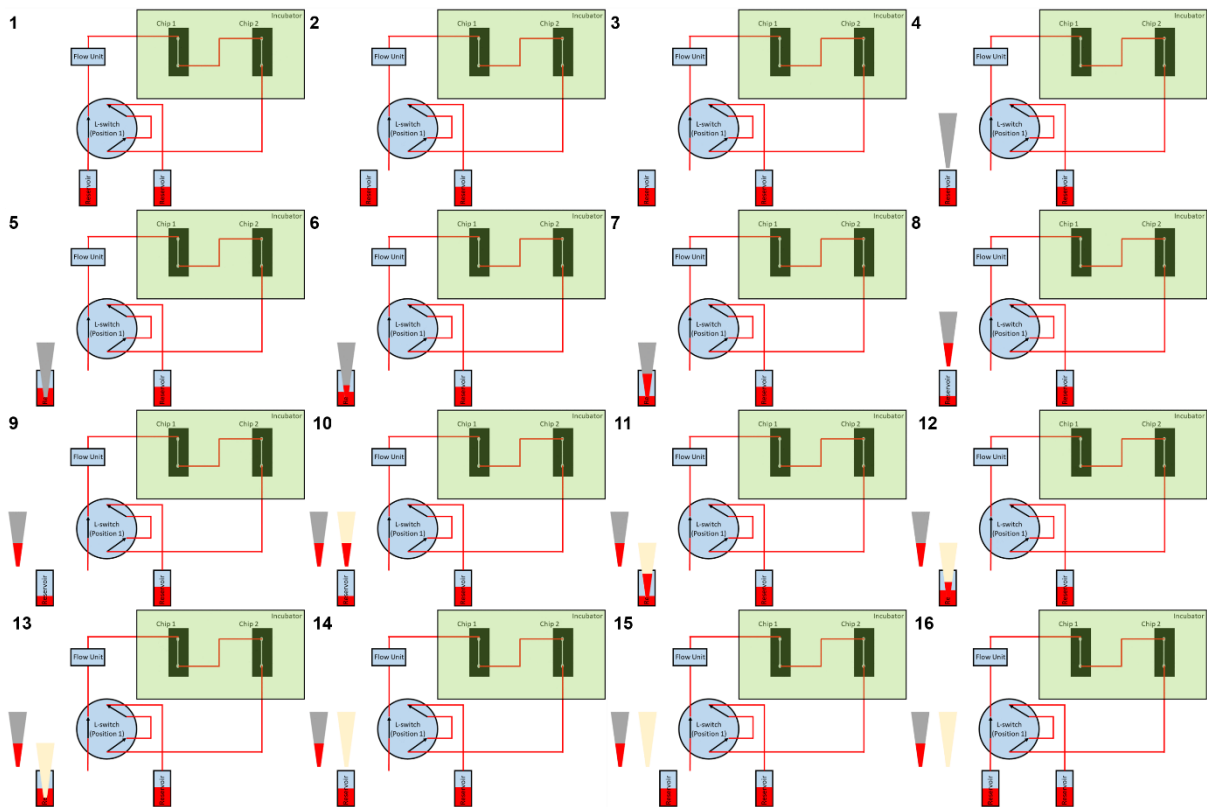
9 Supplementary data



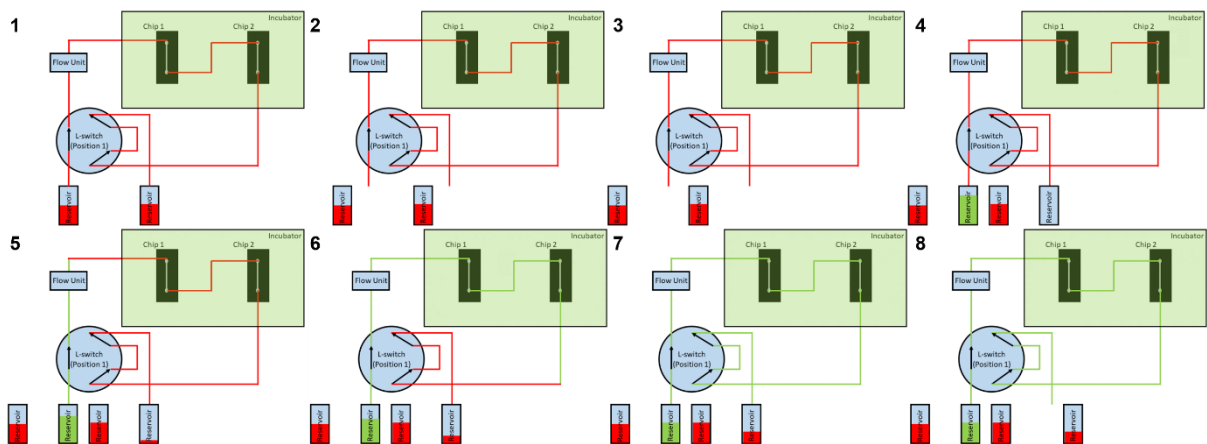
Supplementary Figure 1: Schematical step-by-step overview of a single cycle performed using the fluigent setup. As shown, medium is withdrawn from the left reservoir when the L-switch is in position 1 and vice versa. One cycle takes 25 min when a flow rate of 30 $\mu\text{L}/\text{min}$ is used.



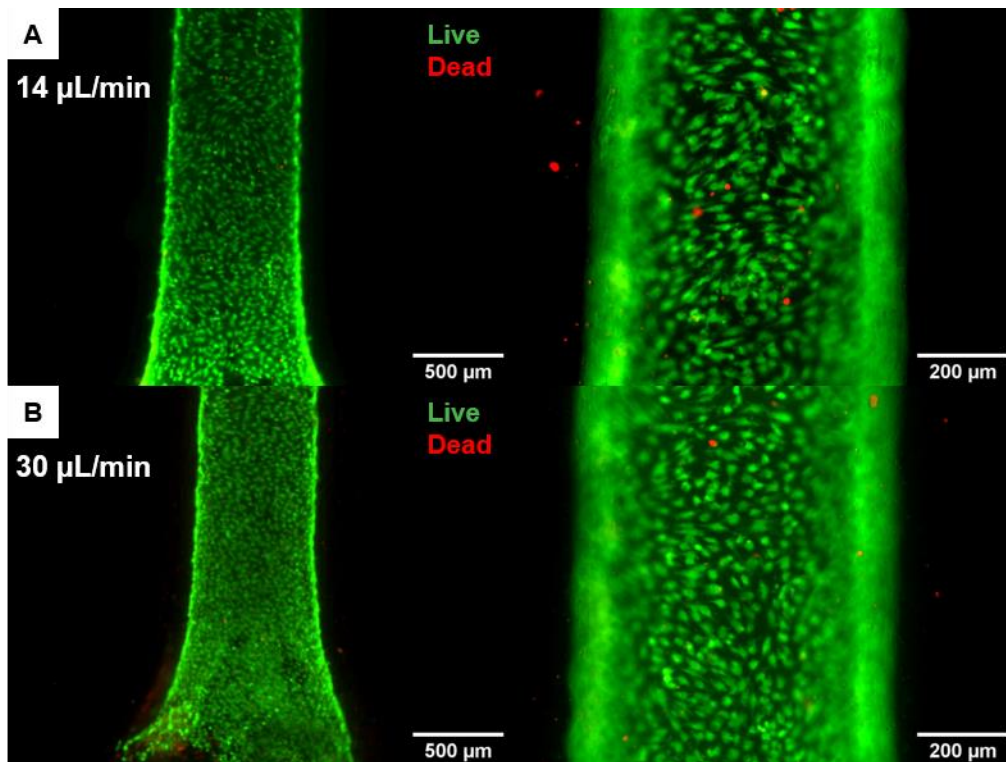
Supplementary Figure 2: Overview of representative flow output results obtained for the circulation when the resistance is too low. Each figure shows ~18 min of circulation with a switch around the 30 minute mark.



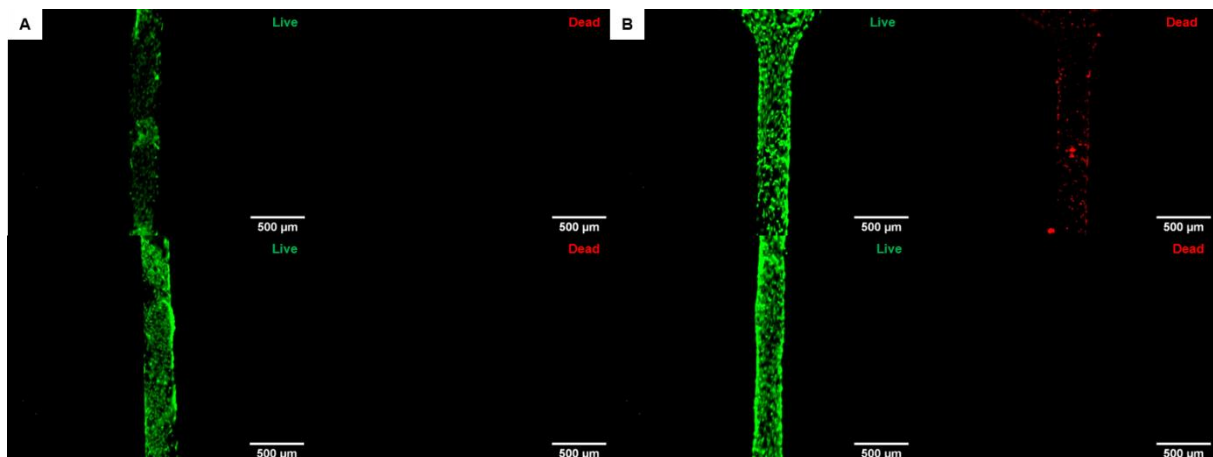
Supplementary Figure 3: Schematical step-by-step overview of routine sampling performed using the fluigent setup. 1-3: After pausing of the circulation, the reservoir is removed. 4-9: A small volume is withdrawn from the reservoir. 10-14: The reservoir is refilled using fresh medium. 15-16: the reservoir is again connected to the circulation and the circulation is continued.



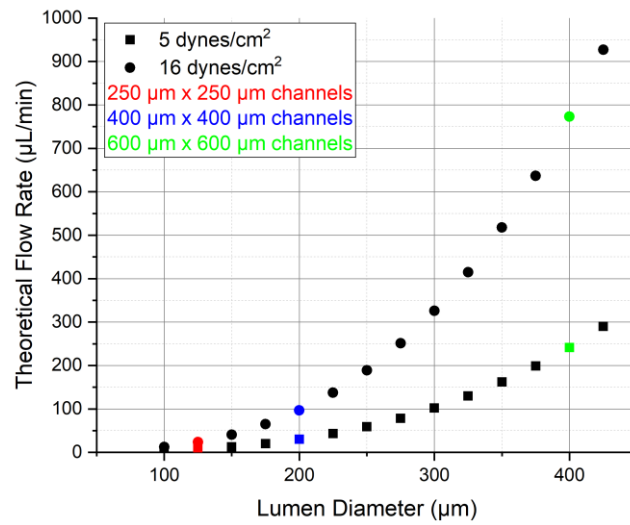
Supplementary Figure 4: Schematical step-by-step overview of final sampling performed using the Fluigent setup. 1-3: Reservoirs are disconnected from the circulation. 4: A new reservoir (containing e.g. PBS or fresh medium) is introduced. 5-7: Fresh volume is flushed through the circulation, whilst collecting the volume left in the circulation. 8: All reservoirs containing "used" medium are disconnected for further analysis.



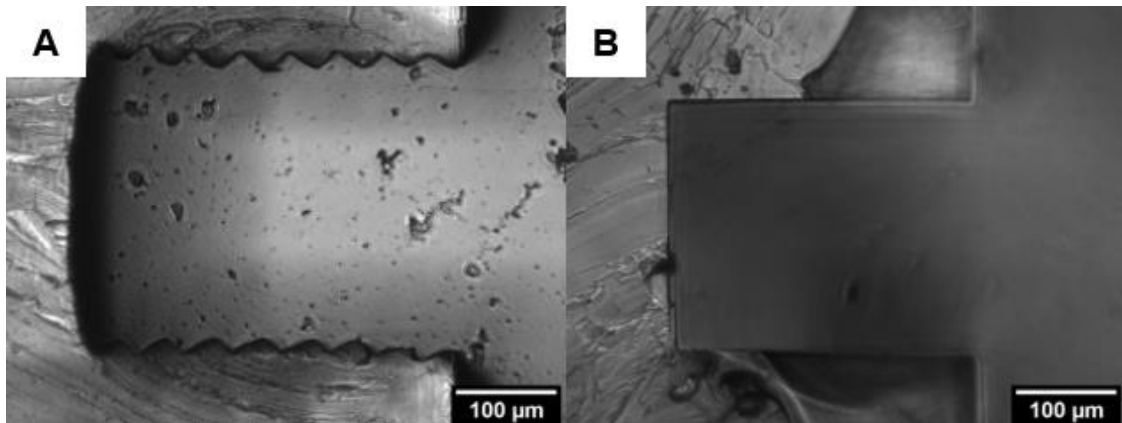
Supplementary Figure 5: HUVECs subjected to 14 $\mu\text{L}/\text{min}$ and 30 $\mu\text{L}/\text{min}$ flow in channels of 600 μm x 600 μm . A: 14 $\mu\text{L}/\text{min}$, and B: 30 $\mu\text{L}/\text{min}$.



Supplementary Figure 6: Overview of HUVEC coated channels used in the circulation for 24 h at 30 $\mu\text{L}/\text{min}$. A: Static control. B: Shear condition.



Supplementary Figure 7: Plot of theoretical flow rate needed to supply lumens of varying diameters with shear stresses of 5 and 16 dynes/cm². In red, theoretical flow corresponding to 250 µm x 250 µm channels (and 125 µm diameter lumens) is shown. In blue, theoretical flow corresponding to 400 µm x 400 µm channels (and 200 µm diameter lumens) is shown. In green, theoretical flow corresponding to 600 µm x 600 µm channels (and 400 µm diameter lumens) is shown.



Supplementary Figure 8: Representative cross-sectional image of channels. A: 3D printed channels (400 µm x 400 µm). B: Channels prepared using SU8 lithography (250 µm x 250 µm).